NBS TECHNICAL NOTE

292

Procedures for Precise Determination of Thermal Radiation Properties November 1964 to October 1965

A Report to: Air Force Materials Laboratory

J. C. RICHMOND, G. J. KNEISSL,
D. L. KELLEY, AND F. J. KELLY

U.S. DEPARTMENT OF COMMERCE
National Bureau of Standards

THE NATIONAL BUREAU OF STANDARDS

The National Bureau of Standards[1] provides measurement and technical information services essential to the efficiency and effectiveness of the work of the Nation's scientists and engineers. The Bureau serves also as a focal point in the Federal Government for assuring maximum application of the physical and engineering sciences to the advancement of technology in industry and commerce. To accomplish this mission, the Bureau is organized into three institutes covering broad program areas of research and services:

THE INSTITUTE FOR BASIC STANDARDS . . . provides the central basis within the United States for a complete and consistent system of physical measurements. coordinates that system with the measurement systems of other nations, and furnishes essential services leading to accurate and uniform physical measurements throughout the Nation's scientific community, industry, and commerce. This Institute comprises a series of divisions, each serving a classical subject matter area:

—Applied Mathematics—Electricity—Metrology—Mechanics—Heat—Atomic Physics—Physical Chemistry—Radiation Physics—Laboratory Astrophysics[2]—Radio Standards Laboratory,[2] which includes Radio Standards Physics and Radio Standards Engineering—Office of Standard Reference Data.

THE INSTITUTE FOR MATERIALS RESEARCH . . . conducts materials research and provides associated materials services including mainly reference materials and data on the properties of materials. Beyond its direct interest to the Nation's scientists and engineers, this Institute yields services which are essential to the advancement of technology in industry and commerce. This Institute is organized primarily by technical fields:

—Analytical Chemistry—Metallurgy—Reactor Radiations—Polymers—Inorganic Materials—Cryogenics[2]—Materials Evaluation Laboratory—Office of Standard Reference Materials.

THE INSTITUTE FOR APPLIED TECHNOLOGY . . . provides technical services to promote the use of available technology and to facilitate technological innovation in industry and government. The principal elements of this Institute are:

—Building Research—Electronic Instrumentation—Textile and Apparel Technology Center—Technical Analysis—Center for Computer Sciences and Technology—Office of Weights and Measures—Office of Engineering Standards Services—Office of Invention and Innovation—Clearinghouse for Federal Scientific and Technical Information.[3]

---

[1] Headquarters and Laboratories at Gaithersburg, Maryland, unless otherwise noted; mailing address Washington, D. C., 20234.

[2] Located at Boulder, Colorado, 80302.

[3] Located at 5285 Port Royal Road, Springfield, Virginia, 22151.

UNITED STATES DEPARTMENT OF COMMERCE • Alexander B. Trowbridge, Acting Secretary
NATIONAL BUREAU OF STANDARDS • A. V. Astin, Director

NBS TECHNICAL NOTE 292

ISSUED FEBRUARY 10, 1967

Procedures for Precise Determination of Thermal Radiation Properties November 1964 to October 1965

J. C. Richmond, G. J. Kneissl,
D. L. Kelley, and F. J. Kelly

A Report to
Air Force Materials Laboratory
Research and Technology Division
Air Force Systems Command
Wright-Patterson Air Force Base, Ohio
Project No. 7381, Task No. 738106
(Prepared Under Contract No. DO (33-615)65-1005)

For sale by the Superintendent of Documents, Government Printing Office
Washington, D.C., 20402 - Price 50 cents

Abstract

The broad overall objective of this continuing program is to develop equipment and procedures for measuring the important thermal radiation properties of materials, particularly those used in aircraft, missiles and space vehicles, at temperatures up to the melting point of the most refractory material, and to develop physical standards for checking such equipment and procedures. During the period covered by this report the specific objectives were (1) continued development of the laser-source integrating sphere reflectometer, (2) an error analysis of the shallow cavity technique for measuring normal spectral emittance, and (3) a study of the feasibility of preparing emittance standards for use at temperatures above 1400 ^{o}K (about 2000 ^{o}F).

An error analysis of the shallow cavity technique for measuring total normal emittance of ceramic materials at very high temperatures showed that there was an error due to the translucency of the specimens that was as much as +60% for alumina, and a second error due to thermal gradients in the specimen that was on the order of -10%. Two new techniques were devised in the hope of greatly reducing the translucency error. Progress was made in developing codes to compute and correct for the thermal gradients present in the specimen. The laser-source integrating sphere reflectometer for measuring reflectance of specimens at very high temperatures was extensively redesigned to eliminate errors due to flux reaching the detector on the first reflection, and to convert the reflectometer from the substitution to the comparison mode. A literature search was made of techniques for measuring thermal radiation properties of solids at temperatures above 2500 ^{o}K (4000 ^{o}F).

Contents

ILLUSTRATIONS

PROCEDURES FOR PRECISE DETERMINATION OF THERMAL RADIATION PROPERTIES

Joseph C. Richmond, Gerhart J. Kneissl, Douglas L. Kelley
and Francis J. Kelly

An error analysis of the shallow cavity technique for measuring total normal emittance of ceramic materials at very high temperatures showed that there was an error due to the translucency of the specimens that was as much as +60% for alumina, and a second error due to thermal gradients in the specimen that was on the order of -10%. Two new techniques were devised in the hope of greatly reducing the translucency error. Progress was made in developing codes to compute and correct for the thermal gradients present in the specimen. The laser-source integrating sphere reflectometer for measuring reflectance of specimens at very high temperatures was extensively redesigned to eliminate errors due to flux reaching the detector on the first reflection, and to convert the reflectometer from the substitution to the comparison mode. A literature search was made of techniques for measuring thermal radiation properties of solids at temperatures above 2500°K (4000°F).

Key Words: Emissivity, emittance, high temperature reflectance, infrared reflectance, radiation properties, reflectance, spectral emittance, spectral reflectance, thermal radiation, total emittance.

1. Objectives

The broad overall objective of this continuing program is to develop equipment and procedures for measuring the important thermal radiation properties of materials, particularly of materials used in aircraft, missiles and space vehicles, at temperatures up to near the melting points of the most refractory materials, and to select, prepare and calibrate physical standards for use by other laboratories in checking their equipment and procedures.

The specific properties of major interest are emittance[1/] and reflectance, and the wavelength range of interest extends from about 0.25μm to 35μm and beyond.

[1/] Emittance is defined as the ratio of the flux per unit area emitted by a specimen to that emitted by a blackbody radiator at the same temperature and under the same conditions.

Work in previous years has been concentrated in the temperature range of room temperature and 800° to 1400°K (about 1000° to 2000°F), and at wavelengths in the 1 to 15μm range.

Specific objectives for the current contract year included (1) continued development of the laser-source integrating sphere reflectometer for measuring reflectance of specimens at high temperature, (2) a study of the errors present in the shallow cavity method of measuring total normal emittance at high temperatures, methods of quantitatively evaluating such errors and/or methods of eliminating them, and (3) a study of the feasibility of preparing emittance standards for use at temperatures above 1400°K (about 2000°F).

2. Shallow Cavity Procedure for Total Normal Emittance

2.1 Background

The equipment for measuring total normal emittance of non-metals by the shallow cavity procedure was designed and constructed on a project sponsored by NASA. Work on this program was transferred to Air Force sponsorship as of November 1, 1964.

2.2 Brief Description of Method

The problem of obtaining reliable thermal emittance measurements on non-metals at temperatures above 1800°K, and particularly above about 2000°K, where standard platinum-base thermocouples cannot be used, has never been solved satisfactorily. Non-metals, and particularly the ceramic oxides, generally have low thermal conductivity, relatively high thermal emittance, and are translucent to appreciable depths below the surface. These properties make it difficult to measure accurately the temperature of an emitting specimen. The combination of high emittance, which also implies high heat transfer rates from the material, and low thermal conductivity tends to produce large thermal gradients in specimens of such materials, and in a specimen that is permitted to radiate from one surface to surroundings at an appreciably lower temperature, the gradients tend to be normal to the emitting surface. The translucency of these materials results in the emitted flux originating in a surface layer of appreciable thickness, rather than from a very thin layer at the surface as in the case of metals and other highly opaque materials. As a further complication, the thickness of this layer will change with the wavelength of the emitted flux, because it is a function of the extinction coefficient of the material, which is wavelength dependent for practically all materials.

When the flux emitted by a specimen originates from a layer of appreciable thickness within which a thermal gradient exists, it is difficult to define the temperature of the emitting volume, and even more difficult to measure it. Even if the effective temperature of the specimen under these conditions is properly defined and measured, the effective temperature of the emitting volume will be wavelength dependent, which is an unsatisfactory situation. In addition, it is extremely difficult to achieve temperature equivalence between a hot specimen and separate blackbody furnace at temperatures above those at which reliable thermocouples are available. An optical or radiation pyrometer measures brightness or radiance temperature, which is the true temperature for a blackbody, but not for real materials. For any specimen, the brightness or radiance temperature must be converted to true temperature, which requires a knowledge of the emittance of the specimen. Since emittance is the property to be measured, such methods of measuring temperature are not very promising.

One method of overcoming the problems inherent in measurements of emittance of non-conductors at very high temperatures is to use an integral blackbody cavity as a reference. If the reference and specimen are at the same temperature, it is not necessary to know that temperature very accurately in order to make accurate emittance measurements. Further, it is possible to make an accurate measurement of the temperature of the blackbody cavity with an optical or radiation pyrometer. The error in emittance measurements arises primarily from the unknown temperature difference between the specimen and reference.

One form of integral blackbody specimen that would appear to offer advantages in measuring the emittance of nonconducting materials at very high temperature is the so-called shallow cavity. This cavity consists of a cylindrical hole of small diameter and shallow depth drilled into the specimen surface. The cavity is on the order of 0.5 mm deep in order to keep the temperature difference between specimen surface and cavity bottom small, so that only a small error will be introduced by assuming isothermal conditions.

A reference cavity of these dimensions is not a very good blackbody. However, if the cavity walls are opaque and reflect diffusely, rather than specularly, if the dimensions of the cavity are accurately known, and if the reflectance and emittance of the cavity wall are the same as for the specimen surface, the measured radiance ratio of specimen surface and cavity bottom can be converted to

emittance. The equation used for this conversion was derived by Gouffé [1][2]. The equation for the emittance of the cavity may be written

$$\epsilon_c = \frac{\epsilon_w [1 + (1 - \epsilon_w)(a/A - f)]}{\epsilon_w (1 - a/A) + a/A} \tag{1}$$

where

ϵ_c = cavity emittance

ϵ_w = emittance of cavity walls

$f = \dfrac{1}{1 + (L/R)^2}$

L = cavity depth

R = cavity radius

a = area of cavity opening

A = cavity surface area including opening

$a/A = \dfrac{1}{2(1 + L/R)}$

We can also write

$$E_t = \frac{L_s}{L_c} = \frac{L_s/L_{bb}}{L_c/L_{bb}} = \frac{\epsilon_s}{\epsilon_c} \tag{2}$$

in which E_t

E_t = radiance ratio of surface to cavity

L_s = normal radiance of specimen surface

L_c = normal radiance of cavity

L_{bb} = radiance of blackbody at specimen temperature

ϵ_s = emittance of specimen

If we assume that $\epsilon_w = \epsilon_s$, we can combine Equations (1) and (2) to obtain

$$\epsilon_s = \frac{E_t (1 + a/A - f) - a/A}{1 - a/A + E_t (a/A - f)} \tag{3}$$

Equation (3) is used to convert the measured radiance ratios into emittance.

---

[2] Figures in brackets refer to references in Section 6.

2.3 Description of Equipment

Equipment for measuring the radiance ratios of shallow cavity specimens was designed and constructed on a contract with NASA. Figure 1 is a drawing of the specimen heater and Figure 2 is a sketch of the optical system.

The specimen is placed in a susceptor heated by induction, or if the specimen is conducting it may act as its own susceptor. Typical specimens are shown in Figure 3. The power is supplied by a 10-kw, 30-MHz radio frequency generator with controlled power output.

The water-cooled field concentrator (Figure 1) is of silver-plated copper. The bell jar is a Pyrex glass pipe cap with the top and the bottom edge ground and polished to provide vacuum-tight seals to the 0-rings. The radiant flux emitted by the hot specimen passes out through a 1/2 inch diameter hole in the top of the bell jar and through a radiation trap and sodium-chloride window to the focusing optical system. The window is mounted at a slight angle to the top surface of the specimen, so that any flux reflected from the window will be trapped, and not impinge on the specimen and thus contribute to the measured flux. The flip mirror above the trap facilitates use of a micro-optical pyrometer for measuring the temperature of the hot specimen. The bell jar is connected to a vacuum system, and has a connection through which an inert gas, such as helium or argon, can be introduced. There is also provision for insertion of a getter filament into the bell jar.

The flux from the hot specimen is emitted vertically, to the focusing optical system (Figure 2), where a plane mirror at 45^{o} to the vertical directs it horizontally to an off-axis ellipsoid, which directs it to a vertical plane mirror which directs it back to the detector, located in the second focal plane. The magnification factor is 2x linear. The detector is mounted on a micrometer stage so that it can be moved both vertically and horizontally in the focal plane. A platinum diaphragm with a small circular aperture, mounted on the detector, restricts the view of the detector to a small selected area of the image of the specimen.

2.4 Brief Outline of Work Performed Prior to November 1964

The validity of the method depends almost entirely upon the validity of Equation (1). In order to assign a value to the accuracy of the measurements, it was necessary to check Equation (1) experimentally. This was done, as is described in detail in a recent paper by Kelly and Moore [2].

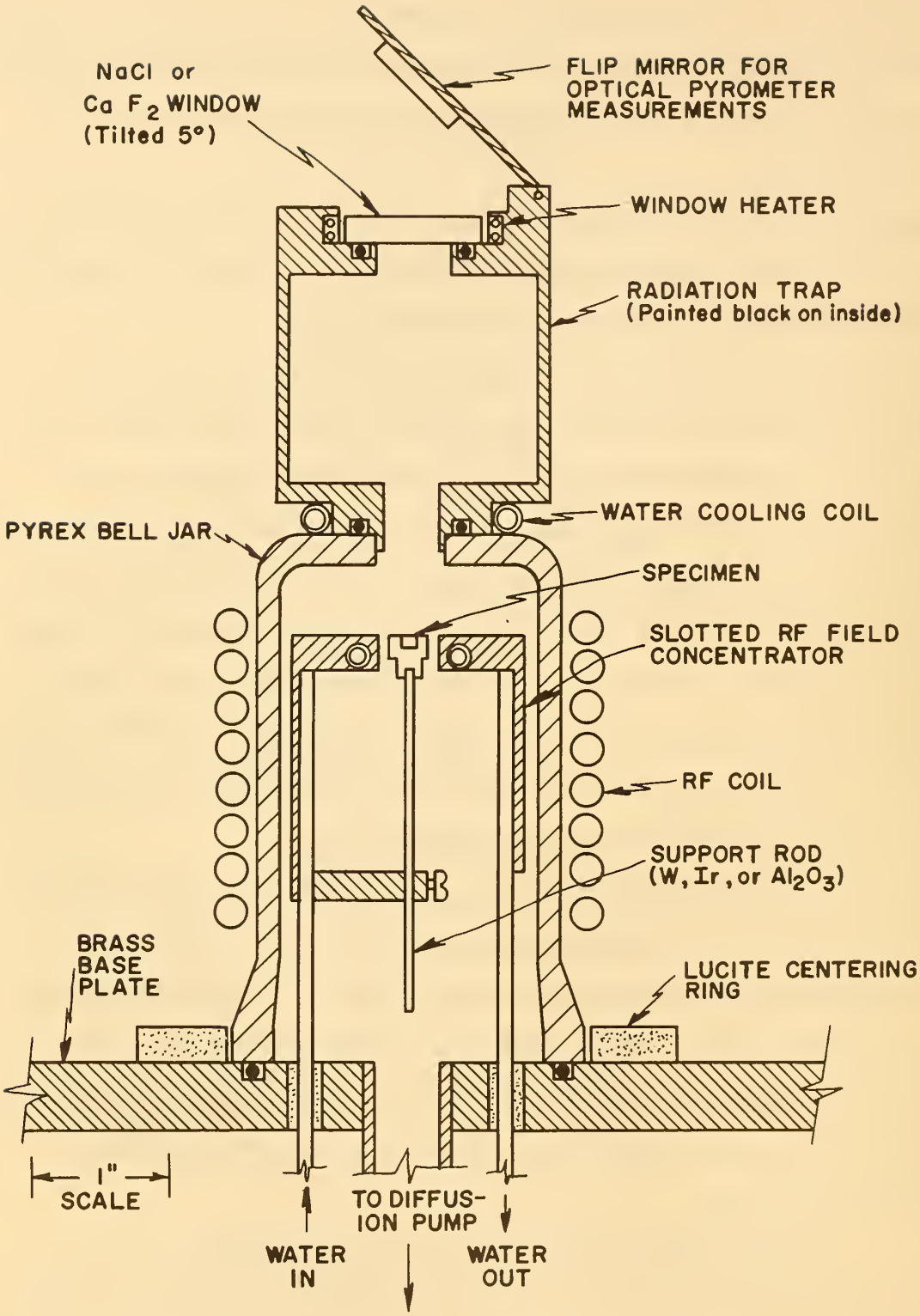

Figure 1. Cross-sectional Drawing of Specimen Furnace

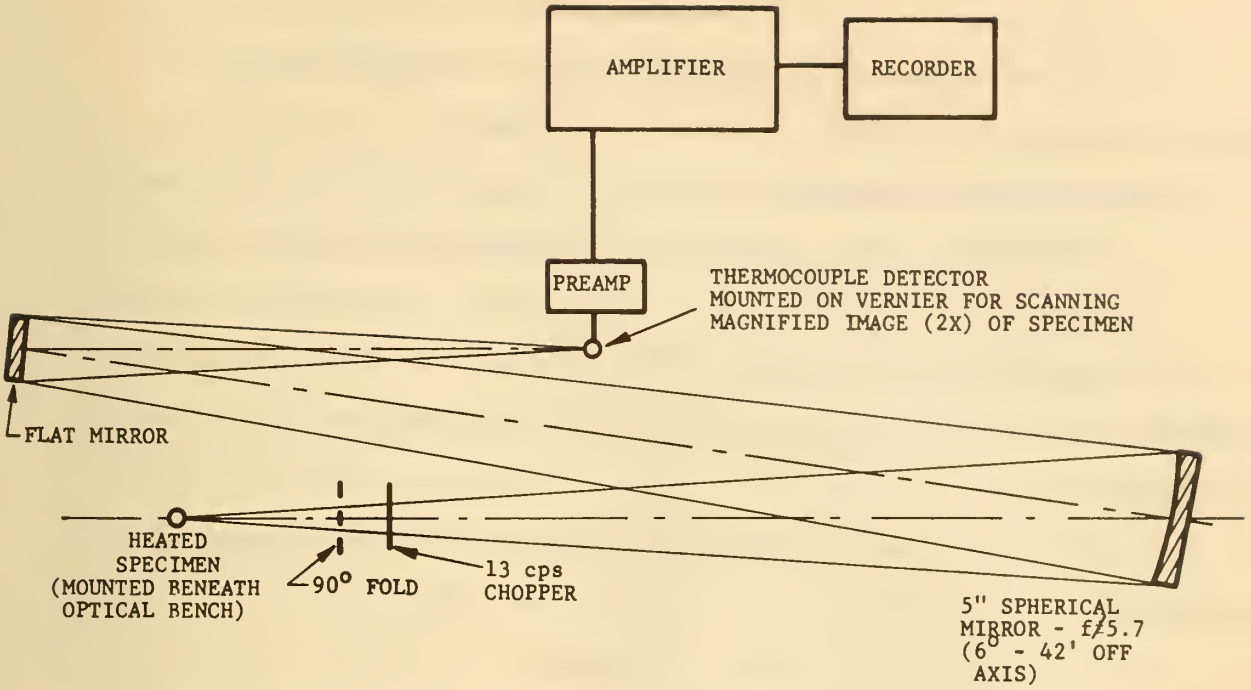

Figure 2. Schematic Drawing of the Optical System.

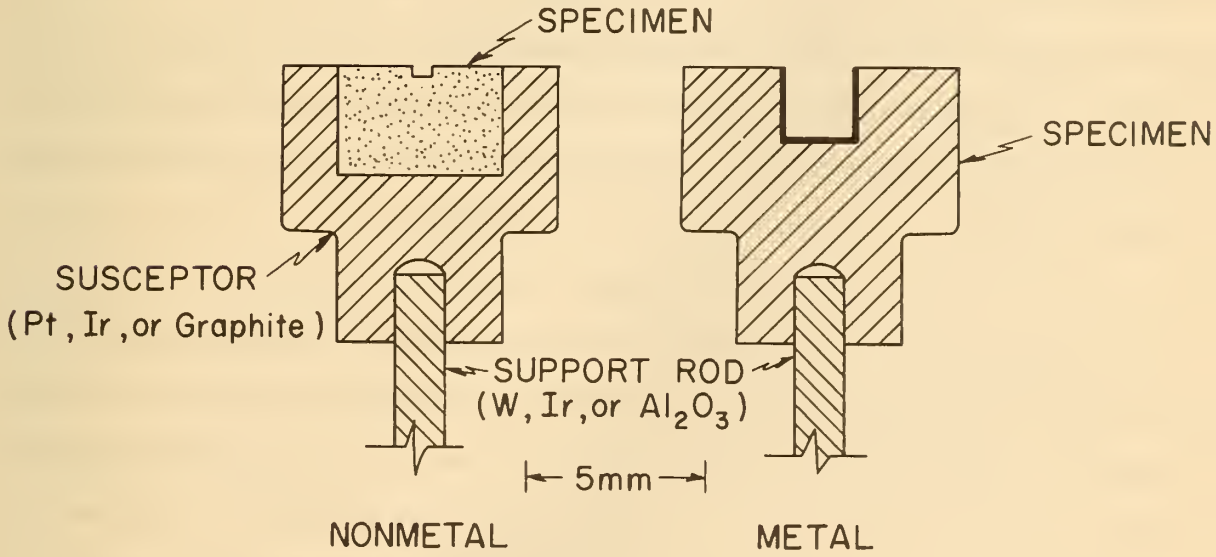

Figure 3. Cross-sectional Drawing of Typical Specimens of Non-Conducting and Conducting Materials

The more important findings were:

(1) When the wall material was a good diffuse reflector, the Gouffé equation predicted the reflectance of shallow-cylindrical cavities to 0.01 in reflectance units.

(2) When the wall material was a somewhat specular reflector (poor diffuser), the equation still predicted with good accuracy (±2%) the reflectance of a cavity with a L/R ratio (depth to radius) of 0.51.

(3) The Gouffé equation can be used to convert measured radiance ratios to emittance without significant error for all materials that are good diffuse reflectors. Fortunately, most non-metals are good diffuse reflectors.

The capabilities of the equipment were demonstrated, and data were obtained on a number of specimens [3].

2.5 Study of Error Sources

Realistic estimates of the errors present in the measurements made with the equipment described above could not be made without separate evaluations. There are several sources of bias in addition to the normal statistical error of measurement. They result primarily from imperfections in the optical system and failure of the experimental conditions to conform exactly to the assumptions on which the Gouffé analysis is based. The three most important error sources can be designated (1) errors due to scattering and aberrations in the optical system, (2) errors due to translucency of the cavity walls, and (3) errors due to thermal gradients.

2.5.1 Optical Scattering Errors

The optical scattering errors result from imperfections in the optical system. The fluxes from the specimen surface and reference cavity pass through the optical system simultaneously. The flux reaching any given small area A' on the image corresponding to the detector aperture will consist of the flux emitted by the corresponding area, A, on the specimen and focused on area A', plus the flux originating from other portions of the specimen or susceptor and deviated to area A' by scattering and imperfections in the optics. In order to evaluate this error, certain basic assumptions must be made:

1). Only small-angle deviations need be considered. Any deviations that cause the emitted flux

to miss the image entirely will be indistinguishable from absorption.

2). The fractions of the flux scattered or absorbed are a function of wavelength, and hence of the wavelength distribution of flux in a measurement of total normal emittance, and the relative sizes of the specimen, cavity and detector aperture. Even though these fractions are wavelength-dependent, they will not change appreciably from one material to another if the wavelength distribution of emitted flux does not change appreciably. These fractions are independent of the flux density.

3). The net effect of the small angle deviations is an increase in the measured radiance due to scattered radiation reaching the detector from areas other than that being directly observed. Flux from the susceptor, specimen and cavity is scattered over the entire image. The contribution of the cavity to the total scattered flux will be small, because the ratio of cavity area to specimen area is about 0.01. Thus the cavity contribution will be only 1 to 2 percent of a total error that is on the order of 5 percent of the measured value. No significant error will be introduced by ignoring the cavity contribution to the total error.

On the basis of the above assumption, the error term can be related to the "true" radiance of the specimen surface for specimens that can be heated directly by induction. Some of the emitted flux is lost in the system, due to absorption, scattering and aberrations. From assumption (2) above, the fraction a, of the flux emitted by area A of the specimen will be focused on the detector, when A is the area of the detector aperture projected through the optical system onto the specimen. The fraction (1 - a) of the emitted flux is lost. Flux will also reach the detector from all other points on the specimen. If s is the fraction of the surface radiance that reaches the detector by scattering, the correction factor for both surface and cavity is $sA'GL_s$ where A' is the area of the detector aperture (which determines the solid angle subtended to the aperture from the specimen) L_s is the radiance of the specimen surface, and G is the total area of the specimen. The measured ratio, E, is then

$$E = \frac{aA'L_s + sA'GL_s}{aA'L_c + sA'GL_s} \qquad (4)$$

setting $K = \frac{sG}{a}$,

$$E = \frac{L_s (1 + K)}{L_c + KL_s} \tag{5}$$

or $EL_c = L_s (1 + K - EK)$. Since $E_t = \frac{L_s}{L_c}$, then $E_t = \frac{E}{1 + K(1 - E)}$ (6)

All that remained was to evaluate the constant K, the scattering factor, in order to evaluate the true radiance ratio, E_t, from the measured E.

It can be seen in Equation (5) that if the cavity can be made nonradiating, $L_c = 0$, then K can be evaluated. The cavity was, in effect, made nonradiating by replacing it with a hole of the same diameter completely through the specimen, and placing a cooled, nonreflecting surface below the hole. Under these conditions any flux reaching the detector when it is focused on the hole must be scattered from the specimen surface. When $L_c = 0$, Equation (5) reduces to $E = (K + 1)/K$. If we designate the radiance ratio measured under these conditions as E_o, then

$$K = (E_o - 1)^{-1} \tag{7}$$

The factor K was found to be about 0.05 for a specimen of oxidized Inconel of the diameter of a normal susceptor as shown in Figure 3, with a 0.5 mm hole, and using a diaphragm with a 0.6 mm hole over the detector.

The factor K is primarily a geometric function of the specimen size, cavity size, and detector-aperture size. It may also be influenced to some extent by the specimen temperature, and probably to a much lesser extent by the spectral emittance of the specimen. It should be independent of the total emittance. The value of 0.05 should be typical for the conditions quoted.

The above analysis is based on the assumption that the amount of scattered flux reaching the detector is the same whether the detector is focused on the center cavity or on the specimen. This assumption was checked by preparing a nickel specimen with two 0.5 mm holes completely through it. One hole was at the center of the specimen, and the other was midway between the center and edge. No significant difference in the amount of scattered flux was detected when the detector was focused

alternately on the two holes, regardless of the orientation of the specimen.

In the more general case, illustrated for the nonmetallic specimen in Figure 3, there will be a hot susceptor surrounding the specimen and some of the scattered flux reaching the detector may originate from the susceptor. An attempt was made to block out such scattered flux by baffling in the optical system, but without success.

This case can be analyzed by the same procedure used for deriving Equations (4), (5) and (6). In this case

$$E_1 = \frac{aA'L_s + sA'GL_s + s'A'G'L_u}{aA'L_c + sA'GL_s + s'A'G'L_u} \tag{8}$$

where s' is the fraction of the susceptor radiance that reaches the detector by scattering, E is the measured-radiance ratio, G' is the area of the susceptor, and L_u is the radiance of the susceptor. All other terms are as in Equations (4), (5) and (6). If we set K' = s'G'/a,

$$E_1 = \frac{L_s(1 + K) + K'L_u}{L_c + KL_s + K'L_u} \tag{9}$$

The two constants can be evaluated as before. In this case K is found by heating a specimen-sized sample with a cavity-sized hole. The radiance ratio, E_o, of cavity flux to surface flux is measured, and K is computed from Equation (7). K' is found by heating a susceptor-sized sample with a specimen-sized hole, and the radiance ratio, E_o, is measured, and K' is computed from Equation (7).

The true radiance ratio, $E_t = L_s/L_c$, is required for substitution in Equation (3) to obtain the emittance of the specimen. Solving Equation (9) for E_t gives

$$E_t = \frac{E_1 - K' L_u/L_c (1 - E_1)}{1 + K - KE_1} \tag{10}$$

The ratio L_u/L_c is required to solve Equation (10). This is the true ratio of susceptor radiance L_u to cavity radiance L_c. The measured value of this ratio, E_2, is given by

$$E_2 = \frac{aA'L_u + sA'GL_s + s'A'G'L_u}{aA'L_c + sA'GL_s + s'A'G'L_u} \tag{11}$$

or

$$E_2 = \frac{L_u\ (1 + K') + KL_s}{L_c + KL_s + K'L_u} \tag{12}$$

solving for L_u/L_c

$$\frac{L_u}{L_c} = \frac{E_2 - K\ (L_s/L_c)\ (1 - E_2)}{1 + K' - K'E_2} \tag{13}$$

but $L_s/L_c = E_t$, thus

$$\frac{L_u}{L_c} = \frac{E_2 - KE_t\ (1 - E_2)}{1 + K'\ (1 - E_2)} \tag{14}$$

substituting the above in Equation (10) gives

$$E_t = \frac{E_1 - K'\ (E_2 - E_1)}{1 + K\ (1 - E_1) + K'\ (1 - E_2)} \tag{15}$$

The correction factor K was evaluated for an oxidized-nickel specimen of the same diameter as a normal nonmetallic specimen, having a cavity-sized hole through its center. A value of 0.113 was obtained. A similar evaluation of K' was made on an oxidized-nickel specimen of the same diameter as a normal susceptor, having a specimen-sized hole through its center. A value of 0.016 was obtained. These values are considered to be typical for any specimen and susceptor combination, and will be used to correct measured total emittances for the scattering error by use of Equation (15).

2.5.2 Translucency Errors

2.5.2.1 Theoretical Analysis

The basic equation for attenuation of flux in traversing a material is $I = I_0\ e^{-kx}$ (16)

where I is the radiant intensity after traversing a thickness x of the material, I_0 is the radiant intensity at x = 0, e is the base of natural logarithms and k is the extinction coefficient. The extinction coefficient is made up of the absorption coefficient α and the scattering coefficient S,

$$k = \sqrt{\alpha\ (\alpha + 2S)} \tag{17}$$

The absorption coefficient α is large for opaque materials, such as metals, but is generally much lower for nonmetallic materials such as ceramic oxides. The absorption coefficient for such

materials varies markedly with wavelength, from a low value at short wavelengths to a high value at long wavelengths. The transition usually occurs rather abruptly, and is called the absorption edge. For most ceramic materials, the absorption edge occurs in the 3-8 micron range.

The absorption coefficient α is a property of a material, and is strongly influenced by minor constituents, lattice defects, etc. The scattering coefficient S is primarily a function of the physical state of the material--grain size, porosity, etc.

A highly opaque material has a high absorption coefficient, and hence all of the incident flux penetrating the surface will be absorbed within a very thin surface layer, and all of the internally generated flux that is emitted will originate within this same very thin surface layer. The thickness, r, of this layer is somewhat indefinite, because as Equation (16) shows, the absorption is an exponential process. About 5% of the initial flux will remain after traversing a thickness of material of 3/k, and about 1.8% after traversing a thickness of 4/k. On this basis, an arbitrary value of $r = 3/k$ is not unreasonable. When k is large, r is so small that no appreciable error is introduced by considering the processes of emission, reflection and absorption to occur at the surface. Essentially all of the flux emitted by an infinitesimal area of surface will originate in the material below that area, and essentially all of the reflectance will occur at the material-air interface.

For translucent materials, r is large enough that emission, reflection and absorption can no longer be considered to occur only at the surface. The flux emitted at an infinitesimal area on the surface of a specimen will originate within a spherical volume of the material with radius r centered at the infinitesimal area, and the flux incident on the plane surface of a specimen in an infinitesimal area will be internally scattered within the material and emerge from a circular area of radius r centered on the incident area.

Since the Gouffé analysis is based on the assumption that the walls of the cavity are opaque, the translucency of the specimen will introduce an error. The shallow-cavity method is based on measurement of the radiance ratio of two areas on the specimen. One area, A in Figure 4, is at the center of the bottom of the shallow cavity, and the other, B, of equal size, is on the flat top of the specimen. The radiance of area A is due to the flux emitted from area A, that emitted by the walls of the cavity and reflected from A, and that emitted by the bottom of the cavity, reflected from the walls

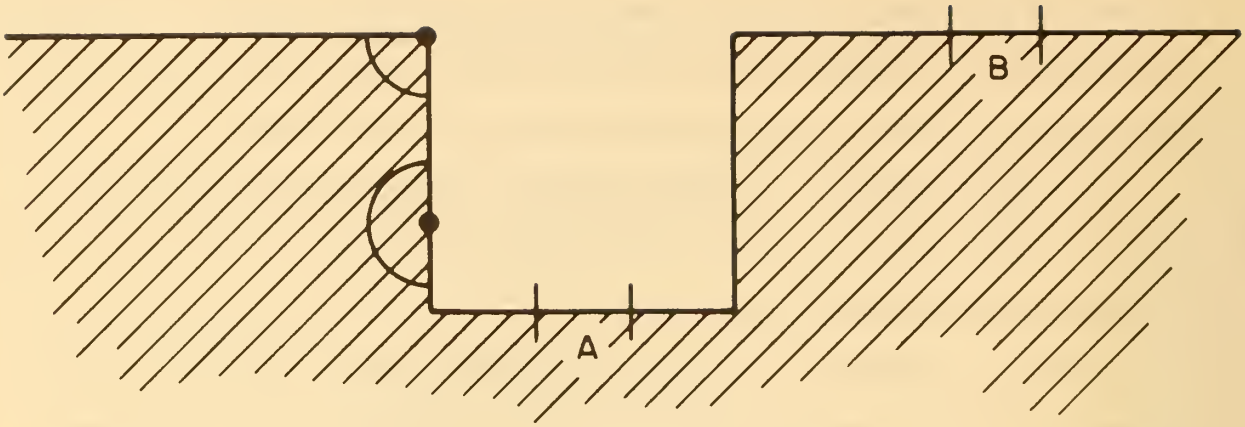

Figure 4. Cross-section of the Shallow Cavity of a Ceramic Specimen.

to A and reflected by A. The radiance of area B is due solely to flux emitted from area B.

Figure 4 shows two infinitesimal areas on the side of the cavity and the spherical volumes of radius r surrounding these areas from which the emitted flux will originate. The flux incident on the indicated areas will be reflected from the area bounded by the intersection of the cylindrical-cavity wall and the sphere of radius r.

It can be seen intuitively from Figure 4 that if r is less than the distance from area B to the cavity or edge of the specimen, the radiance of area B will not be affected by the translucency, and the directly emitted portion of the radiance of area A will not be affected. The emittance and reflectance of an infinitesimal area on the cavity wall will be reduced in a ring of height r below the top of the cavity, by a fraction that approaches 1/2 as the area approaches the top of the cavity, and the radiance of the top of the specimen will be affected within a circular band of width r surrounding the cavity.

The effects of translucency can be summarized as follows: (1) the reflectance of a band of width r at the top of the cavity will be reduced, (2) the emittance of a band of width r at the top of the cavity will be reduced, (3) the emittance of a circular band of width r surrounding the cavity will be reduced, and (4) the apparent emittance of the circular band of width r surrounding the cavity will be

increased due to flux incident on the cavity wall that is transmitted by the specimen and emitted in the circular band. Effects (3) and (4) are compensating, and are small when the volume of the cavity is small, and hence will be ignored, since area B is usually separated from the cavity by a distance greater than r.

The measured radiance ratio, E, can be related to the true radiance of the cavity, L_c, and the specimen L_s as

$$E = \frac{L_s}{L_c - \gamma - \eta} \tag{18}$$

where γ is the correction for the flux not emitted by the band at the top of the cavity, and η is the correction for the decreased reflectance of the band at the top of the cavity. The net effect is that the measured L_c is low. The two corrections are related, and can be combined into a single correction factor, g.

$$E = L_S/(L_C - g) \tag{19}$$

As $r \to 0$, $g \to 0$, or more realistically, $g \to 0$ as $r \ll L$, where L is the depth of the cavity.

2.5.2.2 Experimental Procedure

The experimental procedure used to evaluate g in equation (19) is based on the assumption that the normal spectral emittance measured with the rotating cylinder equipment [4] is essentially free from errors that are present in the values obtained by the shallow cavity technique. This assumption appears to be valid, because in the rotating cylinder method the radiance of a specimen, heated under conditions such that there is essentially no thermal gradient normal to the surface, is measured and compared to that of a laboratory blackbody furnace at the same temperature and under the same conditions. If the rotating cylinder method measures the true normal spectral emittance of a material, the data can be integrated to obtain the true normal total emittance, ε_{tt}. Then if the specimens for the two methods are identical in composition and surface finish, the difference in the measured values can be taken as the error of measurement in the shallow cavity technique.

The error of measurement evaluated by comparison of the rotating cylinder and shallow cavity values would be made up of the scattering error, the translucency error and the thermal gradient error. The scattering error can be separately evaluated and corrected for, as discussed previously.

However, the translucency error and the thermal gradient error are expected to be opposite in sign, and cannot be separately evaluated by these measurements alone.

It is possible, by means of selective filters, to measure the normal emittance of the shallow cavity specimen over a wavelength band where the specimen is translucent, and hence where the translucency error would be expected to be large, and also at another wavelength band where the specimen is essentially opaque, and hence where the translucency error would be very small or completely absent. In this way, by assuming that the thermal gradient error is independent of wavelength (this is only a crude approximation at best), the two error terms can be separately evaluated.

Two filters were used to separate the flux emitted by an alumina specimen into two portions, as mentioned above. The spectral transmittances of the filters are shown in Figure 5. Filter f_1 is of fused quartz, and has high transmittance at wavelengths from the ultraviolet out to about 4.2 μm essentially opaque at wavelengths beyond about 4.6 μm. It thus transmits over the wavelength range where many ceramic materials are translucent. The second filter, f_2 is opaque at wavelengths shorter than about 7.3μm, and has high transmittance from about 7.9 to 14.3μm, where most ceramic materials are essentially opaque.

The normal total emittance of an alumina specimen was measured at 1600°K with no filter in the optical path, and then with filters f_1 and f_2 respectively, in the path. The measured emittances were corrected for the scattering error, by the procedure that was previously described. The normal spectral emittance obtained on a specimen of the same material by the rotating cylinder method at 1600°K was used to compute the true total normal emittance of the alumina at 1600°K by use of the following equation

$$\epsilon_{tt} = \frac{\Sigma_{\lambda_1}^{\lambda_2} I_{b\lambda} \epsilon_\lambda \tau_\lambda \Delta\lambda}{\Sigma_{\lambda_1}^{\lambda_2} I_{b\lambda} \tau_\lambda \Delta\lambda} \qquad (20)$$

where ϵ_{tt} is the "true total" normal emittance of the alumina, $I_{b\lambda}$ is the spectral radiance of a blackbody at 1600°K, ϵ_λ is the normal spectral emittance of alumina at 1600°K, τ_λ is the transmittance of the filter (f_1 or f_2) used (when no filter is used $\tau_\lambda = 1.00$ at all wavelengths) $\Delta_\lambda = 0.5\mu m$, since the products were computed at 0.5μm wavelength intervals, and λ_1 and λ_2 include all wavelengths at

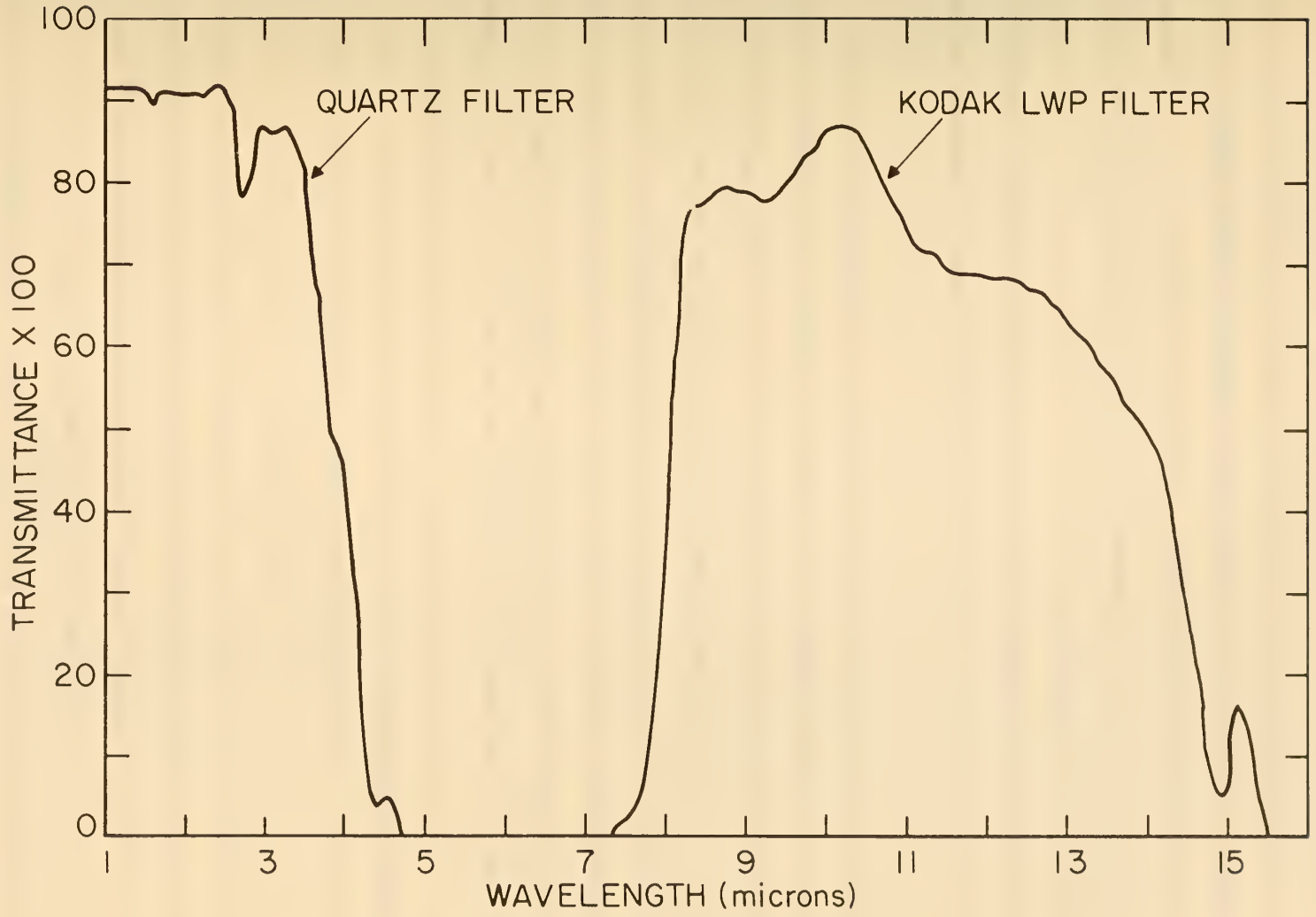

Figure 5. Spectral Transmisttance Curves for Fused quartz and Kodak LWP Filters

which $L_{b\lambda}\tau_{\lambda}$ is significant.

The "true total" emittance, ϵ_{tt}, computed from the normal spectral data, was 0.25 for the case where no filter was used, 0.08 when the quartz filter (f_1) was used, and 0.94 when the Kodak LWP filter (f_2) was used. The values measured with the shallow cavity equipment were 0.31 with no filter, 0.17 with the quartz filter (f_1) and 0.86 with the LWP filter (f_2). All values were corrected for the scattering error, as previously discussed.

The error at the long wavelengths (f_2 filter) was about 8.5% of the "true" value, and is considered to be due almost entirely to the thermal gradients that were present. A temperature difference of about 33°K could account for this error, if total emittance were being measured, in which case the total radiance of a blackbody, $L_{b,t} = \frac{\sigma}{\pi} T^4$, where σ is the Stefan-Boltzmann constant, $\pi = 3.14159$, and T is absolute temperature. Since filter f_2 transmits only in the 7.3 - 14.3μm range, the radiance in this wavelength range from a blackbody at 1600°K is more nearly approximated by $L_b(f_2) = (\sigma/\pi)T^{0.9}$. On this basis, the temperature difference is on the order of 150°K. Such a temperature difference would cause the readings in the short wavelength region to be low by about 38%. On this basis, the error observed in the readings with the f_1 filter of +53% would be made up of a +91% error from translucency and a -38% error from the temperature difference. The readings with no filter had a net error of +24%, which would be made up of an error of about +61.5% from the translucency, and -37.5% from the temperature difference. These errors are intolerably large unless accurate corrections can be made.

2.5.3 Temperature Difference Error

2.5.3.1 Discussion

A basic assumption in the derivation of the Gouffé equation is that the specimen is at uniform temperature. This is at best only an approximation, even for materials of high thermal conductivity and low emittance. When a cylindrical specimen is heated from the bottom and sides, and cooled from the top, there will be a temperature drop from the outside to the center of the cylinder (a radial thermal gradient) and a temperature drop from the hot end to the cold end (an axial thermal gradient). The presence of the cavity at the center of the cooled end causes some slight perturbation of the gradients.

If only the radial thermal gradient were present, the cavity would be cooler than the area of the specimen surface viewed in an emittance measurement, and the measured emittance values would be too high. If only the axial thermal gradient were present, the bottom of the cavity would be hotter than the top and hotter than the area of the specimen surface viewed in an emittance measurement, and the measured emittance would be too low. Thus the effects of the two gradients tend to compensate each other. Preliminary measurements indicate that the axial gradient is much larger than the radial gradient, and that the net effect is to give a measured emittance that is too low. The effect is more complex than this simple analysis would indicate, however. The gradients produce two different effects.

First, since the cavity walls are not isothermal, the cavity would not emit as a blackbody even if it were completely enclosed. There would be net radiant heat transfer within the cavity, and the spectral distribution of flux in the cavity would be different from that in an otherwise identical isothermal cavity. This is not too serious for total emittance measurements, since the detector measures only the total amount of flux emitted, and not its spectral distribution. However, it implies that an effective temperature of the non-isothermal cavity must be defined as the temperature of an otherwise identical isothermal cavity having the same radiance. This effective temperature will be somewhat lower than the actual temperature of the bottom of the cavity, but not as low as that of the top of the cavity wall.

Second, the effective temperature of the cavity will be higher than that of the area of the specimen surface viewed in an emittance measurement. The percentage error from this source will be approximately equal to four times the percentage difference in absolute temperatures of specimen and cavity.

The problem of correcting for the temperature difference error involves first an evaluation of the thermal gradients, and then computation of the effective temperature of the cavity.

2.5.3.2 Thermal Gradient Computations

Several possible methods of computing the thermal gradients in the shallow cavity specimens were considered, and a finite-difference approach was selected as the most promising. In this method, the specimen is divided into a fixed number of small volumes called nodes, the exact number

selected being determined by the accuracy desired and the time available for computation. A temperature is assigned to each node and the heat transfer between each node and each of the surrounding nodes is computed. If the net heat transfer to or from a node is not zero, its temperature is adjusted to reduce the net heat transfer, and the computations are repeated until a temperature distribution is found for which all of the net heat transfers are zero. The thermal gradients are then computed from the temperature distribution.

It should be noted that radiant heat transfer is involved for nodes with exposed surfaces. When nodes view other nodes, as on the interior surface of the cavity, multiple reflections are involved, which will be discussed in more detail.

Various schemes have been used in the past for calculating the heat transfer within a diffusely reflecting and emitting cavity. All of these methods somehow reduce to the solution of N linear equations of N unknowns--or its equivalent--the inversion of an N x N matrix. The procedures involved in radiant transfer calculations are well known; however, the clarity of the concepts involved may perhaps be enhanced when they are expressed in terms of transformations on an N-dimensional vector space. See Appendix I.

2.5.3.3 Results of Thermal Gradient Computations

The temperature distribution in a specimen of simple geometry, shown in Figure 6, was computed by hand. Since the specimen has complete symmetry about the axis corresponding to the center of the cylinder, the thermal gradients in the three-dimensional specimen can be represented in a two dimensional network. The temperature of volumes 5 through 10 were set at 2000°K, and the specimen was assumed to emit to a heat sink at 0°K. Under these conditions, the temperature of a volume is fixed when the total heat flux, by conduction and radiation into the volume, exactly equals that out of the volume. Four simultaneous equations in four unknowns can be set up for the four volumes, as follows:

$$0 = s_i = \frac{A_i \epsilon^2 \sigma}{\rho} \sum_{j=1}^{4} P_{i,j} T_j^4 + \sum_{j=1}^{4} \frac{kA_{i,j}}{h_{i,j}} (T_j - T_i) \qquad (21)$$

$$(i = 1, \cdots 4)$$

where the subscripts i and j refer to the i-th and j-th volumes respectively. (In this case i and j are the numbers of any two of the volumes 1 through 4). ϵ is the emittance, ρ is the reflectance and k is the thermal conductivity of the material. σ is the Stefan-Boltzmann constant. A_i is the exposed surface area of volume i, $A_{i,j}$ is the contact area between volumes i and j, $P_{i,j}$ is the i, j element of a matrix, P, which is similar to the F matrix discussed previously, T is absolute temperature, and $h_{i,j}$ is the distance between the centers of the i and j volumes.

The four unknowns in the equations are T_1, T_2, T_3, and T_4. The equations are rather complex for direct solution, and are most easily solved by a relaxation or iteration procedure. The first step is to arbitrarily assign values to the T_i's, and compute the s_i's. The s_i's represent the net heat transfer to the respective volumes, and are called residuals. A positive s_i indicates that there is net heat gain by the i volume, and that its temperature is too low for its environment; a negative s_i indicates that there is net heat loss by the i volume, and that its temperature is too high for its environment. The volume having the largest $|s_i|$ is farthest from equilibrium. The temperature of this volume is adjusted in predetermined small increments until $|s_i|$ reaches a minimum. Then all of the s_i's are recomputed, using the new T_i for volume i and the old T_i's for all other volumes. This process is repeated until all s_i's are at a minimum. At this point, a change in any T_i by the preselected increment will increase the thermal imbalance in the system. It is then highly probable that the computed T_i's are within a few increments of the values that would satisfy equation (21) exactly.

The temperatures of elements 1 through 4 were computed by hand for the specimen shown in Figure 6. The temperatures of elements 5 through 10 were fixed at 2000°K, and the specimen was assumed to have an emittance of 0.3, a reflectance of 0.7 and a thermal conductivity of 0.42 Joules $cm^{-2}sec.^{-1}(^{o}K\ cm^{-1})^{-1}$, typical values for alumina. The results are shown in Table 1.

A computer code was written to perform the same computation, and after some de-bugging, the same results were obtained, as indicated in Table 1.

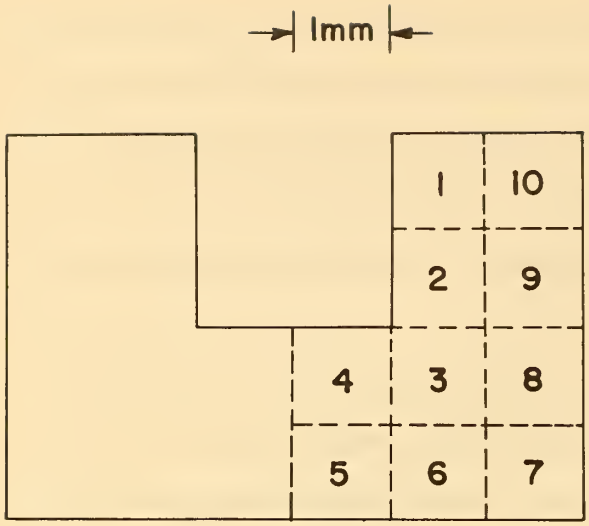

Figure 6. Cylindrical Geometry Used in Trial Calculation of Heat Transfer in a Cavity

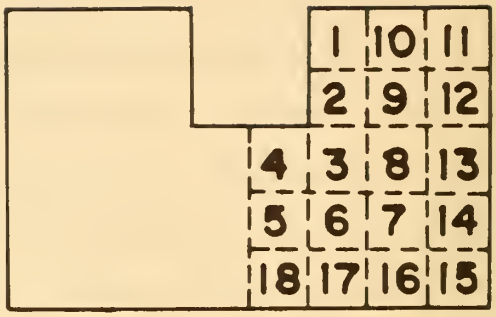

Figure 7. Cylindrical Specimen with Shallow Cavity, Having 18 Nodes

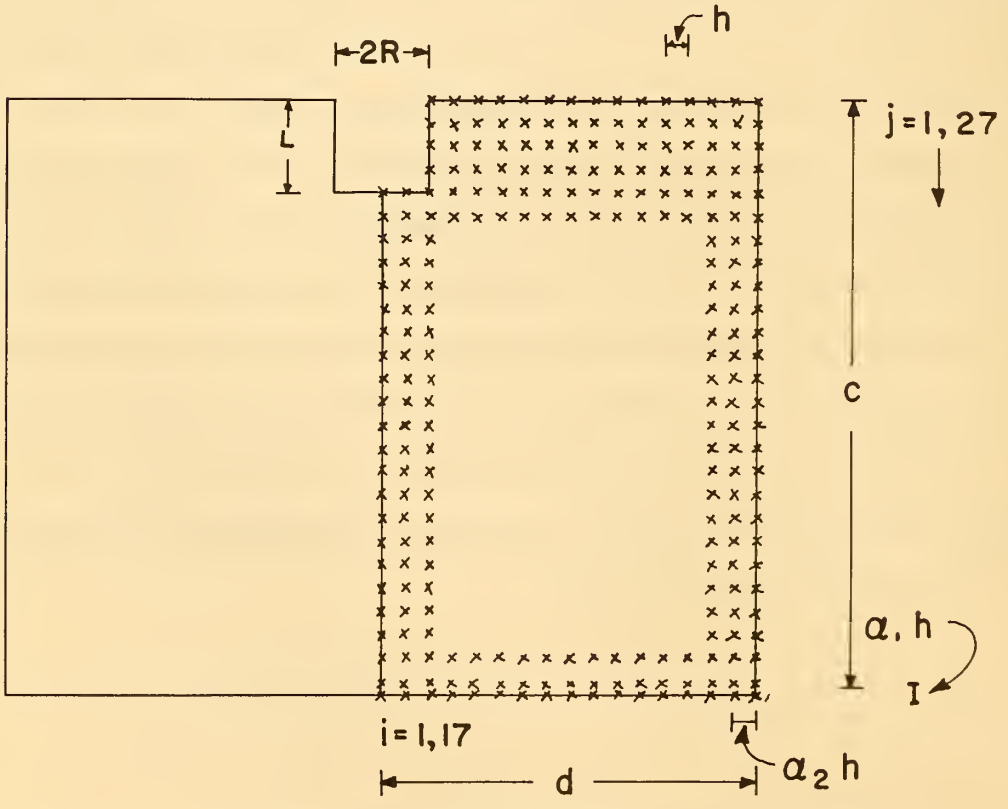

Figure 8. Cylindrical Specimen of Radius d and Length c Containing a Shallow Cylindrical Cavity of Radius R and Length L

Table 1

Temperature Distribution for Specimen Shown in Figure 6.

	Hand & Computer Code
T_1	1958°K
T_2	1981°K
T_3	1993°K
T_4	1987°K

The number of incremental volumes was then increased to 18, with the geometry shown in Figure 7. The same values of ϵ, ρ and k were used as before, and the temperatures of elements 11 through 18 were fixed at 2000°K. The temperatures obtained with the computer are given in Table 2.

Table 2

Temperature Distribution for Specimen Shown in Figure 7.

T_1	1903°K	T_6	1987°K
T_2	1944°K	T_7	1991°K
T_3	1972°K	T_8	1983°K
T_4	1967°K	T_9	1966°K
T_5	1985°K	T_{10}	1925°K

It is obvious from a comparison of the data in tables 1 and 2 that the number of elemental volumes must be greatly increased before the computed temperature distributions will approach those encountered in real specimens. It will be noted in Figure 7 that elements 3, 5, 6, 7, 8 and 9 have no exposed surface area, hence A_1 in equation 21 is zero, and the first term drops out. Under these conditions equation 22 can be used to compute thermal gradients within the specimen. This equation expresses the temperature T at a point r, z within a cylinder in terms of the radial distance r from the center axis of the cylinder and the vertical distance, z, from the top end of the cylinder. The equation is

$$\frac{\partial^2 T}{\partial r^2} + \frac{1}{r}\frac{\partial T}{\partial r} + \frac{\partial^2 T}{\partial z^2} = 0 \qquad (22)$$

and applies when steady state heat transfer exists in the specimen. The boundary conditions at the surfaces of the specimen must be supplied in order to solve equation 22. A computer code is being developed to solve the equation, based on the geometry of Figure 8. The code will be general in form, so that it can be applied to other specimen configurations to be discussed later.

In order to solve equation 22 by a finite difference approach, a series of node points must be located throughout the specimen, and the temperature at each node must be written in terms of the temperatures of the surrounding nodes. Each node represents a volume that surrounds it, having dimensions, in the plane shown, extending half way to each surrounding node.

For any specimen having complete axial symmetry, the thermal gradients can be represented in a two-dimensional lattice, as in Figures 6 and 7. Such a generalized lattice is shown in Figure 8, in which the nodes are spaced a distance h apart on a aquare lattice, in the c and d directions, parallel to and normal to the specimen axis, respectively. Each node is identified by an i, j index, in which i represents the column, numbered outward from the specimen axis, and j represents the row, numbered downward from the top of the specimen. For the lattice shown it is assumed that the depth L and radius R of the cavity are evenly divisible by h, but that the height c and radius d of the specimen are not necessarily divisible by h. When the dimension d is not evenly divisible by h, the distance between i_{max} and i_{max}-1 will be some fraction α_1 of h, and when the dimension c is not evenly divisible by h the distance between j_{max} and j_{max}-1 will be some fraction α_2 of h.

There will be a separate equation relating the temperature of each node to the temperatures of the surrounding nodes. These equations will be similar for nodes with similar surroundings. Hence it is convenient to divide the lattice into zones such that the same equation applies to all of the nodes in that zone. In order to describe these zones mathematically, the following symbols will be used.

$i_{cav.}$ = The i-index of the column of nodes on the cavity wall

$j_{cav.}$ = The j-index of the row of nodes on the cavity bottom

i_{max} = The i-index of the column of nodes on the outer specimen wall

j_{max} = The j-index of the row of nodes on the specimen bottom

The eleven regions can be described as follows:

R1 - $i < i_{max}$, $j = j_{max}$ - These are the nodes on the specimen bottom.

R2 - $1 < i < i_{max} - 1$, $j = j_{max} - 1$ - These are the nodes in the row immediately above the specimen bottom, except for the node at the center and the two nodes at the outer surface.

R3 - $i = 1$, $j_{cav} < j < j_{max} - 1$ - These are the nodes in the center column, at least two rows above the specimen bottom and below the cavity bottom.

R4 - $i \leq i_{cav}$ and $j = j_{cav}$, or $i = i_{cav}$ and $j \leq j_{cav}$. These are the nodes on the cavity wall.

R5 - $i < i_{cav}$ and $j < j_{cav}$. These are the nodes inside the cavity. Since these nodes are in air or free space, it can be considered that they do not exist.

R6 - $i_{cav} < i < i_{max}$, $j = 1$. These are the nodes on the top of the specimen.

R7 - $i = i_{max}$ and $1 \leq j \leq j_{max}$. These are the nodes on the outer surface of the specimen.

R8 - $i = i_{max} - 1$, $1 < j < j_{max} - 1$. These are the nodes in the first row in from the outer surface of the specimen, below the top row and at least two rows above the bottom.

R9 - $i_{cav} < i < i_{max} - 1$, $1 < j < j_{max} - 1$ or $1 < i \leq i_{cav}$, $j_{cav} < j < j_{max} - 1$. These are the nodes in the interior of the specimen at least a distance h from the top and axis of the specimen and cavity walls, and at least a distance 2 h from the specimen bottom or side.

R10 - $i = i_{max} - 1$ and $j = j_{max} - 1$. This is the node just inside the bottom outside corner of the specimen.

R11 - $i = 1$, and $j = j_{max} - 1$. This is the node in the next to the bottom row along the axis of the specimen.

The equations that apply in these regions are as follows:

R1 - No equation - all nodes in this region are assumed to be at the same predetermined temperature.

$$R2: \quad T_{i,j} = 0.5 \left[\frac{\alpha_1}{\alpha_1 + 1}\right] \left\{T_{i-1,j} + T_{i+1,j} + \frac{h}{2R_i}\left[T_{i+1,j} - T_{i-1,j} + \frac{2}{\alpha_1(\alpha_1 + 1)}\right]\left[\alpha_1 T_{i,j-1} + T_{i,j+1}\right]\right\} \tag{23}$$

$$R3: \quad T_{1,j} = \frac{2}{3} T_{2,j} + \frac{1}{6}\left[T_{1,j-1} + T_{1,j+1}\right] \tag{24}$$

R4: $\underset{\sim}{k}\frac{\partial T}{\partial n} = F\ \epsilon\sigma\underset{\sim}{T}^4$ (25)

R5: There is no specimen material at the location of the nodes, hence no equation is required.

R6: $T_{i,1} = \left[-\frac{k}{h} - 4\epsilon\sigma(T'_{i,1})^3\right]^{-1}\left[3\epsilon\sigma\,(T_{i,1})^4 - \frac{k}{h}\,T_{i,2}\right]$ (26)

R7: Nodes in this region are at the same predetermined temperature as those in region R1.

R8: $T_{i,j} = \frac{2\alpha_2 R_i}{2\alpha_2 R_i + 4R_i - h(\alpha_2 - 1)}\left\{T_{i,j+1} + T_{i,j-1} + \right.$ (27)

$\left.\frac{2}{\alpha_2(\alpha_2 + 1)}\,(\alpha_2 T_{i-1,j} + T_{i+1,j}) + \frac{1}{2\alpha_2 hR_i}\,(-\alpha_2 T_{i-1,j} + T_{i+1,j})\right\}$

R9: $T_{i,j} = \frac{1}{4}\left[T_{i+1,j} + T_{i-1,j} + T_{i,j+1} + T_{i,j-1}\right] +$ (28)

$\frac{h}{8R_i}\left[T_{i+1,j} - T_{i-1,j}\right]$

R10: $T_{i,j} = \frac{2\alpha_1\alpha_2 R_i}{4R_i(\alpha_1+\alpha_2) - h\alpha_1(\alpha_2 - 1)}\left\{\frac{2}{\alpha_1(1+\alpha_1)\,\alpha_2(1+\alpha_2)}\right.$ (29)

$\left[\alpha_1\alpha_2(1+\alpha_1)\,T_{i-1,j} + \alpha_1\alpha_2(1+\alpha_2)\,T_{i,j-1} + \alpha_1\,(\alpha_1+1)\,T_{i+1,j} + \right.$

$\left.\left.\alpha_2\,(1+\alpha_2)\,T_{i,j+1}\right] - \frac{\alpha_2\,T_{i-1,j} - T_{i+1,j}}{2\alpha_2 hR_i}\right\}$

R11: $T_{i,j} + \frac{\alpha_1}{2\alpha_1 + 1}\left[2T_{2,j} + \frac{\alpha T_{i,j-1} + T_{i,j+1}}{\alpha_1(\alpha_1+1)}\right]$ (30)

In the above equations, $T'_{i,j}$ is the temperature of the i, j node on the previous iteration. $R_i = h(i-1)$, and $\partial T/\partial n$ is the vector thermal gradient normal to the surface. All other terms have been defined previously.

The computation of the temperature distribution in a specimen by this procedure requires the simultaneous solution of i j equations in i j unknowns. This is obviously impossible except by computer techniques. Again an iterative technique is used, as was previously explained. This method of solving the conductive heat transfer problem has been used many times in the past with good results [5].

Some progress has been made in preparing a computer code to perform the above computation, but much work remains to be done.

2.6 New Procedures

Because of the large errors found in the shallow cavity technique, two new techniques were developed that use the same basic equipment, but for which the errors were expected to be much smaller.

The new techniques involve comparison of the flux emitted by the hot specimen to that emitted by (1) a comparison standard of known emittance, at the temperature of the specimen, or (2) by a deep cavity in the specimen that approaches a blackbody radiator. These will be referred to as the center post and deep cavity techniques. Both techniques require a specimen in the form of a thick walled cylinder, of the same outside diameter as the shallow cavity specimen, and an inside diameter slightly larger than that of the cavity in the shallow cavity specimen.

2.6.1 Center Post Technique

In the center post technique the susceptor has a center post of the same diameter as the center hole in the specimen, as shown in Figure 9. The top of the post is flat, and serves as the comparison standard of known emittance. The center post also performs a second function in heating the specimen, and thus reducing the thermal gradients. The center post is both a good thermal conductor and a good electrical conductor. Heat is conducted by the post from the outer susceptor to the specimen, and heat is generated by induction in the post itself.

The material first chosen for use as the susceptor with the center post technique was high-purity graphite.* This material was chosen because of its high melting point, good electrical properties, high opacity and high emittance. Tests showed that it worked very well at temperatures of 1400 and 1600°K, but that it reacted with or diffused into the ceramic specimens at higher temperatures.

Tungsten was next used as the susceptor for the center post technique. It has a very high melting point, good electrical properties, and many measurements of its emittance are reported in the literature. The maximum temperature at which a tungsten susceptor could be used was found to vary with the composition of the specimen being measured.

With the center post technique there is no cavity, and thus the errors due to translucency of the cavity walls and the thermal gradient along the cavity walls will be eliminated. There will still be a

*Mfr. designation ATJ, National Carbon Co.

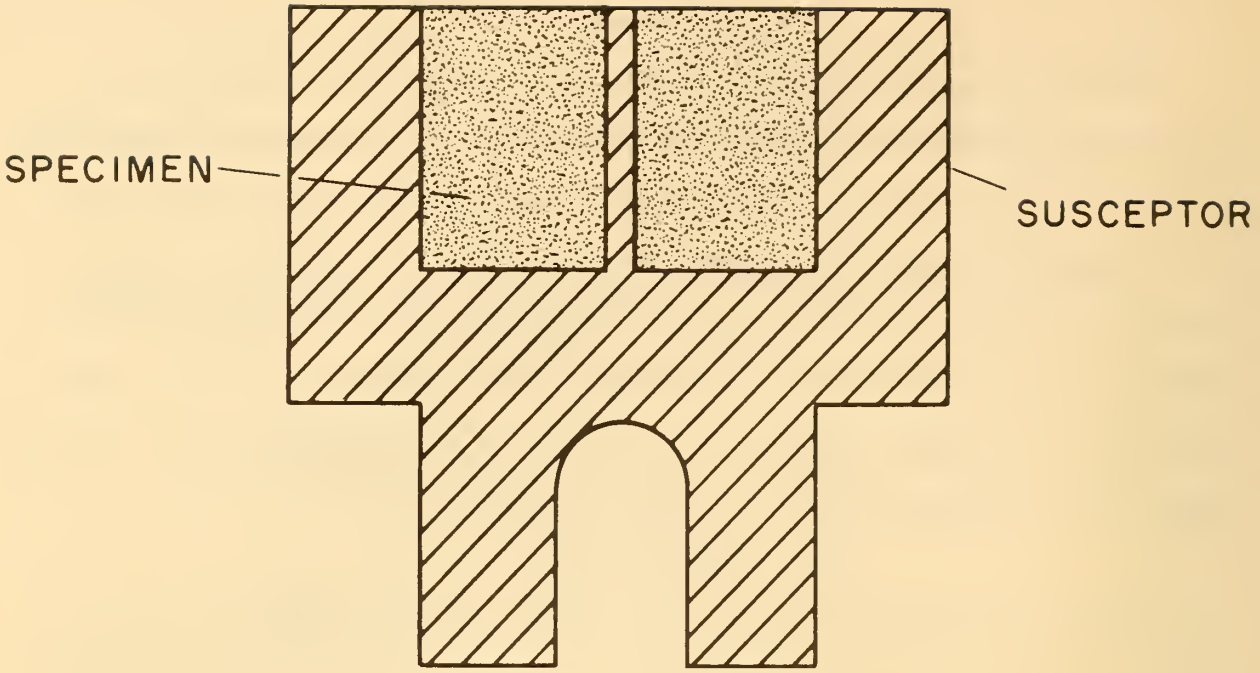

Figure 9. Cross-sectional Drawing of specimen Mounted in Susceptor with Graphite Post Comparison Standard

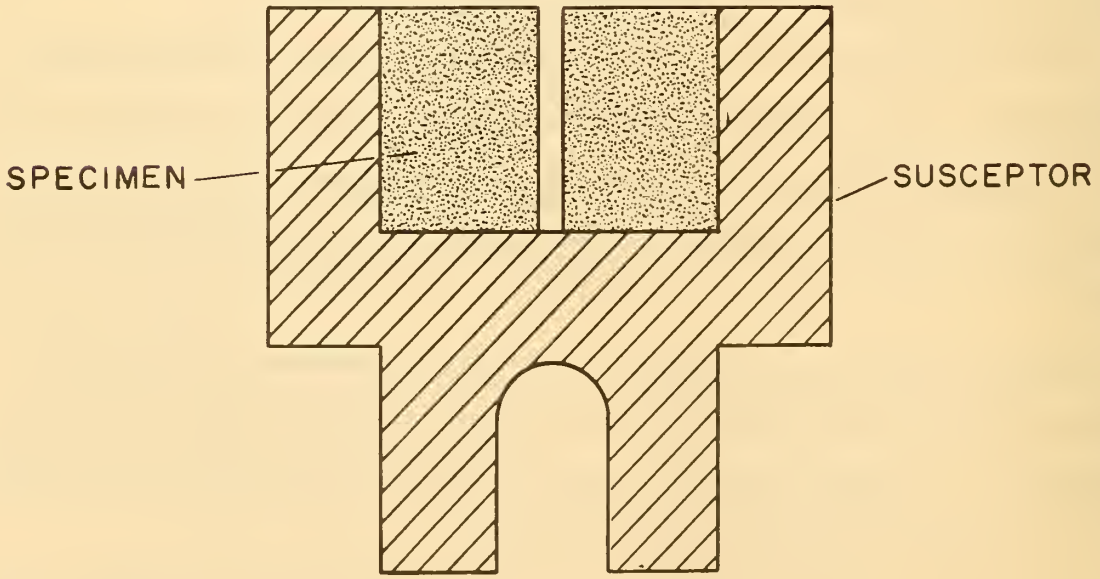

Figure 10. Cross-sectional Drawing of Specimen with Deep Cavity, Mounted in Susceptor

temperature difference between the center post and the area of the specimen viewed for measurement.

If E is the ratio of the specimen radiance to that of the center post, we can write

$$E = \frac{L_s}{L_c} = \frac{\epsilon_s \pi \sigma T_s^4}{\epsilon_c \pi \sigma T_c^4} \tag{31}$$

in which L_s is the normal radiance of the specimen, L_c is that of the post, ϵ_s is the normal total emittance of the specimen and ϵ_c is that of the center post, π and σ are constants which cancel out, T_s is the absolute temperature of the specimen and T_c is that of the center post. Solving for ϵ_s we get

$$\epsilon_s = E \epsilon_c \frac{T_c^4}{T_s^4} \tag{32}$$

If $T_c = T_s$, the only corrections that need be made are those for ϵ_c and the scattering error which has been discussed previously. T_c can be measured accurately with an optical pyrometer, since the normal spectral emittance at the optical pyrometer wavelength of the center post is known. If the corresponding emittance of the specimen is known, T_s can also be measured directly. If it is not known, T_s can be computed by the techniques previously discussed, or estimated by techniques that will be discussed later.

2.6.2 Deep Cavity Technique

In the deep cavity technique a susceptor of the type used with the shallow cavity technique is used, as shown in Figure 10. The cylindrical hole through the specimen forms a deep cavity that is a reasonable approximation of a true blackbody, especially if the bottom of the cavity is of a high emittance material. In this case the normal spectral emittance of the cavity is taken as 1.00, and T_c can be measured accurately with an optical pyrometer. The major uncertainty in this procedure is the evaluation of T_s. The temperature difference between T_s and T_c will be much larger than in either the shallow cavity or center post techniques. It will thus be necessary to correct for the temperature difference error. The translucency error is not completely eliminated by the deep cavity technique, but its magnitude, compared to that for the shallow cavity technique, is greatly reduced. These errors will be discussed in more detail in the following section.

Equation (32) is modified for the deep cavity technique to

$$\epsilon_s = E \frac{T_c^4}{T_s^4} \tag{33}$$

since in this case ϵ_c is assumed to be 1.00.

A graphite susceptor was used for the first measurements by the deep cavity technique. This had a special advantage for this method, because the high emittance of the graphite bottom of the cavity made it a near perfect blackbody. However, graphite had the same disadvantages here as when used with the center post technique - diffusion of graphite into the specimen, and reaction with the specimen, particularly at high temperatures.

Tungsten susceptors were used in the later work. Since tungsten is easily oxidized, it was necessary to work in an oxygen-free atmosphere or in a vacuum of better than 10^{-5} torr. Because of the relatively low emittance and specular reflectance of tungsten, which formed the bottom of the deep cavity, the inside of the cavity was lined with nickel oxide, to increase the emittance and diffuseness of the cavity to a point where it approached a true blackbody. Unfortunately the nickel oxide decomposed at temperatures above about 1800°K, and nickel metal was deposited on the bell jar and sodium chloride window. As a result, measurements by this technique were restricted to temperatures below about 1700°K. Another coating having high emittance plus greater thermal stability in vacuum at high temperatures is being sought.

2.6.3 Discussion of New Procedures

The two new techniques have advantages over the shallow cavity technique in that the only serious errors are the scattering error and the temperature difference error. The scattering error is a function of the optical system, and can be evaluated and corrected for.

The temperature difference error is the largest source of uncertainty in either method. An accurate correction for this error can be made if the temperatures of the specimen at the area viewed, and the temperature of the center post or deep cavity, can be accurately evaluated. The temperature of the center post can be measured with an optical pyrometer, because its normal spectral emittance at the optical pyrometer wavelength is known. That of the deep cavity can also be measured, because its emittance is taken as 1.00.

Evaluation of the temperature of a partially translucent specimen is more complex. Such a

specimen emits from a spherical volume of radius r, within which a thermal gradient exists, as previously explained and illustrated in Figure 4.

The total flux emitted from an elemental area of surface will be made up of the sum of the fluxes originating in elemental volumes within the specimen at distances less than r from the surface element, each emitting at its own temperature. Each of these fluxes is attenuated logarithmically, as indicated in equation 16, in traversing the specimen to reach the surface element. Hence the specimen has no unique temperature at which it is emitting, but rather a range of temperatures, which is determined by the magnitudes of the thermal gradient and extinction coefficient. The extinction coefficient, k, varies with wavelength for most materials.

For any non-isothermal translucent specimen there will exist an effective temperature, which is defined as the temperature of an otherwise identical isothermal specimen that is emitting at the same rate. Such an effective temperature can be computed for the combination of thermal gradient and extinction coefficient that will exist at any one wavelength. The computation becomes more complex when a large wavelength range is involved, over which the extinction coefficient varies widely, as in the case of measurements of total emittance. To further complicate the problem, the extinction coefficient, k, will usually also vary with temperature, although such variations are usually much smaller than the variations with wavelength.

The brightness temperature, measured with an optical pyrometer, of a non-isothermal specimen, is the same as that of an otherwise identical isothermal specimen at the same effective temperature for the optical pyrometer wavelength, as defined above. Also the radiance temperature, measured with a total radiation pyrometer, of such a specimen is the same as that of an otherwise identical isothermal specimen at the same effective temperature for total emitted flux. The brightness temperature or the radiance temperature can be converted to true temperature if the appropriate emittance is known. Unfortunately, however, this is usually not the case, since the total normal emittance is the property being measured.

For most ceramic materials the optical pyrometer temperature will be a better approximation of the effective temperature for total emitted flux than will the surface temperature.

There are then, three basic techniques that can be used to evaluate the effective temperature of

the specimen (1) to compute it by the techniques previously discussed, which requires a knowledge of the thermal conductivity and extinction coefficient of the specimen, (2) to measure it with an optical pyrometer or total radiation pyrometer, which requires a knowledge of the appropriate emittance, or (3) to measure the temperature distribution across the top of the specimen in terms of brightness temperature (optical pyrometer temperature uncorrected for emittance) and assume that the observed differences in brightness temperatures are equal to the corresponding differences in true temperatures. Technique No. 3 is the most easily applied, because it requires no prior knowledge of the properties of the specimen, but it is also probably the least accurate of the three techniques.

The translucency error is largely eliminated in both new techniques. It arises from a net transfer of radiant flux across the interface between the center post or deep cavity and the specimen. If there is net transfer of radiant flux into the specimen, the measured apparent emittance of the specimen will be too high in a ring of width r around the top of the post or cavity, the apparent emittance of the post or cavity will be too low, and the measured emittance will be too high. If the net transfer of radiant flux is in the opposite direction, the measured emittance will be too low.

If the center post was a perfect mirror, there would be no net transfer across the interface, and no error. Also, if the specimen and center post are at the same temperature, there will be no net transfer of flux across the interface. Flux will be crossing the interface in both directions, but the amounts will be exactly the same, because the transmission of the interface along any optical path will be identical in the two directions, and the incident radiance in the two directions will be equal on the two sides. Hence we can say that there is no translucency error in the center post technique.

There is no net transfer of radiant flux across the wall of a blackbody cavity, since by the definition of a blackbody the absorbed flux is exactly equal to the emitted flux. Thus if the deep cavity were a true blackbody, there would be no net transfer of radiant flux across the wall of the cavity, and hence no translucency error. Unfortunately the cavity departs appreciably from blackbody conditions especially near the top of the specimen. The net effect is that there will be net transfer of radiant flux into the cavity from the specimen, and the apparent emittance of the specimen is low in a ring of width r around the top of the cavity. Because of the depth of the cavity the effect of the translucency error on the apparent emittance of the cavity bottom will be negligibly small, and can be ignored.

Thus the net translucency error will be negligible if the portion of the specimen viewed for measurement is more than the distance r from the edge of the deep cavity.

2.7 Total Normal Emittance Measurements

Data were obtained on specimens of four materials by all three techniques, shallow cavity, center post, and deep cavity. So far only the data taken by the shallow cavity method have been reduced and no correction has been made for the translucency error or the temperature difference error. The four materials were alumina, thoria, magnesia and zirconia. The tungsten used for the susceptor was also measured. See Appendix II.

2.7.1 Alumina

The normal spectral emittance of two specimens of alumina was measured at temperatures from 1400 to 1900°K. One specimen had consistently higher emittance than the other, as shown in Figure 11. The average value for the two specimens checks data obtained previously. The alumina specimens were difficult to polish satisfactorily. The individual grains were relatively large and very hard and the bond between grains was relatively weak. As a result there was a tendency for the grains to break loose during polishing, leaving a rough, non-uniform surface. The observed difference in the emittance of the two specimens that were measured is ascribed primarily to the known difference in surface finish of the two specimens, rather than to a difference in composition.

2.7.2 Magnesia

The normal spectral emittance of two specimens of magnesia was measured at temperatures from 1400 to 1800°K. This material is easy to machine, but very fragile. Again a consistent difference was observed in the emittance of the two specimens.

The data shown in Figure 12 agree very well with published values by Olson and Morris [6] and Pears [7].

2.7.3 Zirconia

The normal spectral emittance of three specimens of zirconia was measured at temperatures from 1400 to 1800°K. The tungsten susceptor reacted with the zirconia at temperatures above about 1850°K, causing a reduction of ZrO_2 to Zr metal.

The zirconia has low thermal conductivity and had the largest thermal gradients observed on

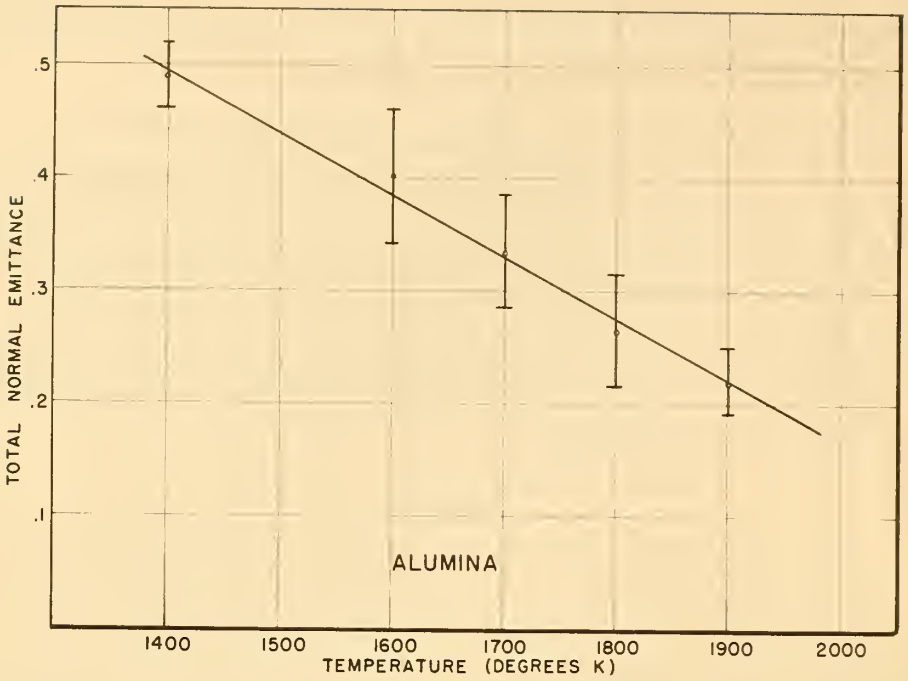

Figure 11. Normal Total Emittance of Alumina, Measured by the Shallow Cavity Technique

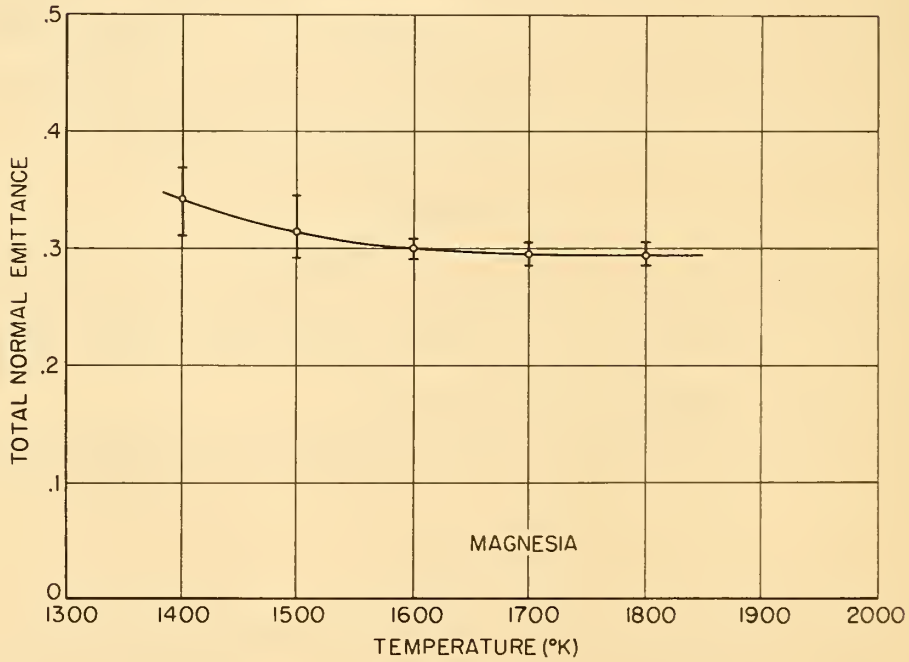

Figure 12. Normal Total Emittance of Magnesia, Measured by the Shallow Cavity Technique

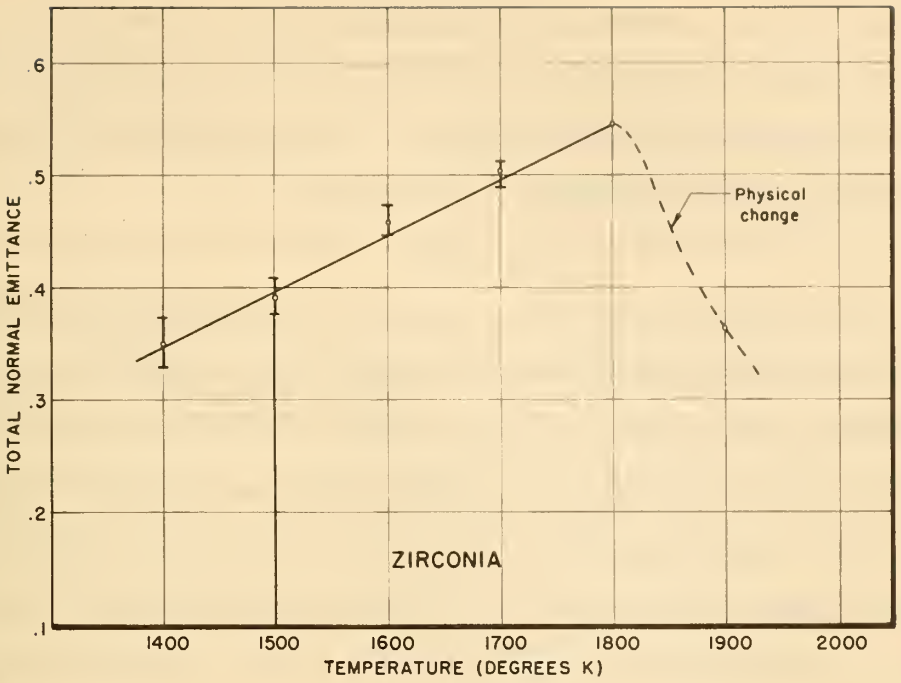

Figure 13. Normal Total Emittance of Zirconia, Measured by the Shallow Cavity Technique

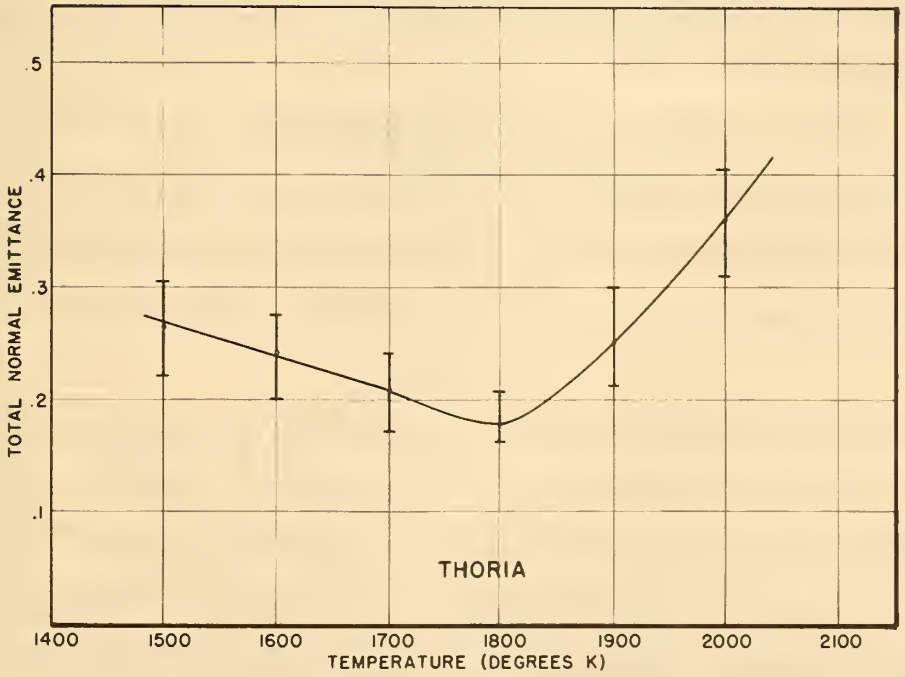

Figure 14. Normal Total Emittance of Thoria, Measured by the Shallow Cavity Technique

any of the four materials tested. Specimens broke if heated too rapidly. The readings from one spot to another on one specimen varied more than for any other material tested but the average values for the three specimens agreed well, as indicated in Figure 13. The data in Figure 13 agree well with results published by Cox [8], Olson and Morris [6] and Pears [7].

2.7.4 Thoria

Measurements were made on four specimens of thoria, at temperatures from 1500 to 2000°K. There was no indication that the specimens would not withstand heating to higher temperatures, but there was not sufficient power available to reach higher temperatures with the available power source. Some fogging of the sodium chloride window of the bell jar enclosing the hot specimen occurred at the temperature of 2000°K, which is believed to be from tungsten oxide produced by reaction of the susceptor with traces of oxygen in the vacuum system, which was at a pressure of about 10^{-5} torr.

The emittance was relatively constant over the surface of any one specimen but there was appreciable variation from specimen to specimen, as shown in Figure 14. The data plotted in Figure 14 agree well with similar data published by Pears [7] at 1500°K, but he reports essentially constant emittance at temperatures from 1500° to 1900°K, with a sharp increase in emittance at higher temperatures.

2.8 Materials for Emittance Standards

The four materials referred to above had been selected as possible candidate materials for use as emittance standards in the 1400-2500°K temperature range (approximately 2000-4000°F). On the basis of experience to date, none of the materials is an outstanding choice for this use.

2.8.1 Alumina

The melting point of alumina is only slightly above 2300°K, but the fact that it is readily available and relatively easy to fabricate make it appear suitable for use as a standard at temperatures up to perhaps 2200°K. The specimens that were tested did not come up to expectations. This may be due to the physical structure of the specimens that were tested, which made it difficult to produce a smooth surface by conventional grinding and polishing techniques, and thus contributed to the observed differences in emittance of specimens that were supposedly identical.

2.8.2 Magnesia

The high melting point, 3073°K, of magnesia would appear to make it suitable for use as a high-temperature emittance standard. It is relatively easy to fabricate specimens by machining since the material is relatively soft. However, it is perhaps too fragile, since it will break with rough handling. The emittance appears to be quite uniform, not only from one point to another on a specimen, but from specimen to specimen.

The major disadvantage of magnesia is its chemical instability. It will react slowly with moisture and carbon dioxide in the atmosphere at ambient temperatures, to form $Mg(OH)_2$ and $MgCO_3$, with an appreciable increase in volume. At high temperatures, above about 1700°K, it reacts with many materials with which it comes in contact, and particularly with the tungsten susceptor. It also has a relatively high vapor pressure at high temperatures. The normal spectral emittance of MgO was found to vary only slightly with temperature in the 1400-1800°K temperature range.

2.8.3 Zirconia

Zirconia is by far the hardest of the materials tested. It is very brittle, and very difficult to machine. As mentioned previously, it has low thermal conductivity, and must be heated and cooled slowly to prevent fracture from thermal shock. It reacts with tungsten at temperatures above about 1800°K. The emittance varies appreciably over the surface of a specimen by as much as 0.25 in emittance. There is some indication that the emittance of the material changes as a result of heating. This is not surprising in view of the known phase change which occurs in the pure material on heating, which is inhibited by the addition of a stabilizer such as CaO.

2.8.4 Thoria

Thoria is relatively easy to machine, and the specimens do not vary appreciably in emittance over the surface. Although there was appreciable variation in emittance from specimen to specimen of those tested, the values for any one specimen were reproducible on repeated measurements. No reaction with the tungsten susceptor was noted at temperatures below 2100°K.

Thoria has another possible disadvantage as a standard because of its slight radioactivity. This requires special precautions on the part of those machining specimens to avoid breathing or ingestion of the dust.

2.8.5 Metals

Of the metals available for use as standards in the 1400-2500°K temperature range, only iridium, molybdenum, niobium, osmium, rhenium, ruthenium, tantalum, and tungsten have melting points high enough to make them suitable for use over the entire temperature range. Of these, iridium and rhenium have better oxidation resistance than the others, and of the readily oxidized metals tungsten has the highest melting point and lowest vapor pressure at high temperatures. On this basis, iridium and tungsten have been selected for further tests.

3. Laser-Source Integrating Sphere Reflectometer

3.1 Background

Reflectance, which is defined as the ratio of reflected flux to incident flux, is nearly independent of temperature, while the emitted flux, which is measured in an emittance determination, is a very strong function of temperature, particularly at wavelengths below the peak of the Planck curve. Hence errors due to errors in temperature measurement should be much smaller in reflectance measurements than in direct measurements of emittance.

The basic problem in measuring reflectance of specimens at high temperatures is to discriminate between the flux reflected by the specimen and that emitted by the hot specimen. The classical method of discriminating is to chop the incident flux, and to use synchronous a. c. amplification of the signal from the detector, which essentially ignores the unchopped flux emitted by the hot specimen. This system is most satisfactory when the a. c. signal from the detector produced by the chopped reflected flux is large compared to the d. c. signal produced by the unchopped emitted flux, and fails completely when the d. c. signal is appreciably larger than the a. c. signal. For this reason conventional thermal sources are not very satisfactory for use in reflectance measurements of specimens at very high temperatures, particularly for measuring spectral reflectance.

A laser emits a high-intensity, highly collimated beam of flux over a very narrow wavelength band and hence should be an ideal source for use in high-temperature reflectance measurements. Preliminary computations show that the 1 mW output of a helium-neon continuous-wave gas laser is equivalent to the flux that would be produced in the same wavelength band by a blackbody radiator at a temperature of about 1,200,000°K.

One disadvantage of the laser source is that it operates at only a few specific wavelengths. However, for materials that do not undergo changes in structure or phase as a result of heating, the general shape of the spectral reflectance curve does not change appreciably with temperature, so that it is possible to interpolate and extrapolate the high-temperature reflectance curve of a material on the basis of accurate measurements made at a few wavelengths and the complete room-temperature reflectance curve.

3.2 Previous Work

The laser-source integrating sphere reflectometer was designed and built to measure spectral directional hemispherical reflectance of specimens at temperatures up to 2500°K. The original 35.5 cm (14 in.) integrating sphere was designed for use in the substitution mode. There was only one sample port, and the specimen and comparison standard were alternately placed over the specimen port for measurement.

Performance tests showed that the error in reflectance measured with the original equipment was on the order of ±0.02 in reflectance units, which for dark specimens was as much as 50% of the measured value, and it was not possible to accurately predict or correct for the error.

The reflectometer reading obtained when a specimen is at the specimen port is related to the reflectance of the specimen, and when the specimen is replaced with a comparison standard of known reflectance, the reading obtained is related to the reflectance of the standard. The assumption is made that the constant relating instrument reading to reflectance is the same for the two cases, so that the reflectance of the specimen is computed by correcting the ratio of observed reflectometer readings for the known reflectance of the standard. The error arises from the fact that the constant relating reflectometer reading to reflectance is a function of the geometric distribution of reflected flux in the integrating sphere.

The detector views a small portion of the sphere wall. If the sphere wall is a perfect diffuser, which it approximates, the same fraction of the flux incident on the viewed area of the sphere wall will always be received by the detector. However, the fraction of the reflected flux that reaches the detector is larger for the flux that is directly incident on the viewed area, and thus reaches the detector after a single reflection from the sphere wall, than for the reflected flux that is directly

incident outside the viewed area, and thus must undergo two reflections from the sphere wall before reaching the detector. The maximum error from this source can be evaluated by comparing readings obtained with a good mirror oriented so that the specularly reflected beam falls, first, entirely inside the viewed area, and second, falls entirely outside the viewed area. The difference between the two readings, divided by the smaller reading, is the maximum possible percentage error from the source. For any specimen the fraction of the reflected flux that is directly incident on the viewed area is a function of the geometric distribution of reflected flux. If this fraction is the same for the specimen and reference standard, there is no error from this source.

3.3 Design Modifications

3.3.1 Requirements

Because of the somewhat disappointing performance, the basic design of the reflectometer was reviewed. The requirements to be met are as follows:

a. The reflectometer should measure reflectance accurately, regardless of the geometric distribution of reflected flux from the sample or comparison standard.

b. The reflectometer should be capable of measuring reflectance in absolute units or relative to a comparison standard.

c. The specimen heater should not disturb the sphere configuration, and should be capable of heating the specimen to at least 2500°K.

d. The reflectometer should be adapted for operation with air, vacuum or inert atmosphere in the sphere.

3.3.2 Sphere Geometry

In order to discuss the modifications of the sphere, it is first necessary to describe its geometry. The sphere is made up of two hemispheres, which are joined with bolted flanges having an 0-ring seal. The principal axis of the sphere is defined as the diameter normal to the plane through the joint connecting the hemispheres. The primary plane of the sphere is defined as the plane containing the principal axis and the center of the entrance port, and the secondary plane of the sphere is defined as the plane through the principal axis and normal to the primary plane. The apex of all angles mentioned is the center of the sphere, and angles are measured from the principal axis.

The entrance port was located in the upper hemisphere, and centered 14° from the principal axis. In the original design the specimen port was located in the lower hemisphere and centered on the principal axis. There were two detector ports, one in each hemisphere. The one in the lower hemisphere was located 60° from the principal axis. Since the two hemispheres could be rotated relative to each other, this port could be positioned in either the principal plane, where it was identified as No. 1, or in the secondary plane, where it was identified as No. 2. The detector port in the upper hemisphere, identified as No. 3, was centered 45° from the principal axis in the primary plane, nearest the entrance port.

3.3.3 Sphere Modifications

The sphere design was modified to permit operation in the comparison mode, as shown in Figure 15. Only the detector port identified as No. 3 was used, and the field of view of the detector was restricted to a small area of the sphere wall diametrically opposite the detector port. The sample specimen port was replaced by two ports, one for the specimen and one for the comparison standard. These ports were located in the lower hemisphere, in the secondary plane, centered 20° on either side of the principal axis. They are thus located symmetrically with respect to the entrance port and detector port.

Shields were introduced into the sphere to prevent reflected flux from impinging directly on the area viewed by the detector. Since the area viewed by the detector is located near the specimen ports, small shields could be used, which do not appreciably disturb the sphere configuration. Because it is sometimes desirable to operate the reflectometer without the shield for the comparison standard, it was attached to the sample holder rather than the sphere itself. A sample holder without the shield can be used if desired.

Restriction of the field of view of the detector to a small area of the sphere which is shielded from the sample eliminates the effects of variations in the geometric distribution of reflected flux on the measured reflectance. All of the flux reflected from the sample must be reflected at least twice by the sphere before reaching the detector. If the sphere surface is a perfect diffuser the reflected flux will be uniformly distributed over the surface of the sphere after the first reflection from the sphere. If the sphere surface is also uniform in reflectance, a constant fraction of the flux that is

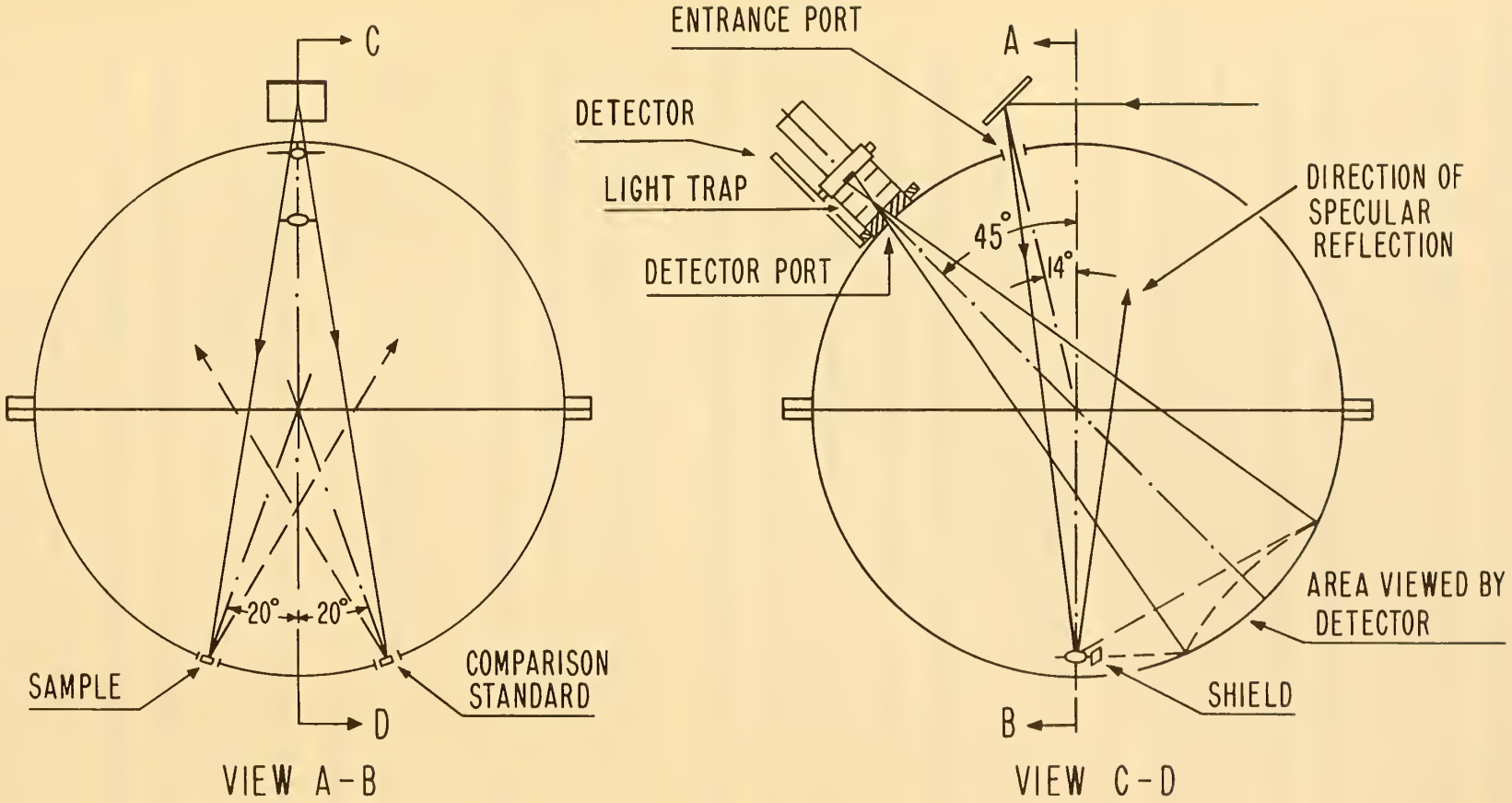

Figure 15. Schematic Views of Sphere Geometry

reflected by the specimen will reach the detector, regardless of its geometric distribution. The barium sulfate coating used on the sphere is uniform in reflectance and is also a very good diffuser at wavelengths shorter than about 2 microns.

3.4 Relative Reflectance Measurements

The modified sphere is well suited to measurement of relative reflectance. This type of measurement will be particularly well suited to evaluation of the thermal coefficient of reflectance. The reflectance of the hot specimen will be measured relative to a nearly identical specimen of the same material at room temperature, and the change in reflectance produced by the change in temperature can be measured directly.

Elimination of the error due to variations in the geometric distribution of reflected flux permits use of a high reflectance mirror as the comparison standard. The absolute reflectance of such a standard can be calibrated very accurately (to about 0.1%) by a multiple reflection technique, hence this procedure can be used to obtain accurate absolute reflectance.

The ratio of the detector outputs when the two specimens are irradiated will be the ratio of their reflectances, to an accuracy of better than 1%. The only errors that have not been eliminated are those due to flux losses out the entrance port and detector port. Such losses are small, being approximately equal to the ratio of the total area of the openings to the total area of the sphere, which is 0.0027. This fraction of the flux reflected by the specimen and standard would be lost, and hence the total error from this source would be appreciably less than the figure quoted. For a specimen and standard with the same geometric distribution of reflected flux the losses would be the same, and the error from this source would be zero.

3.5 Absolute Reflectance Measurements

A literature survey revealed that of the many possible ways to measure absolute reflectance with an integrating sphere reflectometer, that described by McNicholas [9] appeared particularly well suited for use with the present sphere. In this method, the comparison standard is replaced by a spherical cap of the same radius as the sphere, and coated with the sphere coating, but without the shield, so that the area of view of the detector is no longer shielded from the comparison standard. Under these conditions, the ratio of the detector outputs when the specimen and the sphere coating

are alternately irradiated is the absolute reflectance of the specimen.

Let F_o be the incident flux, A_o the area viewed by the detector, A the total area of the sphere, ρ_s the directional hemispherical reflectance of the specimen, ρ_w the reflectance of the sphere wall, and $L'(\theta',\varphi')$ the reflected radiance in the direction $\theta'\varphi'$.

Flux F_o is incident on the specimen from the direction θ,φ. The reflected flux incident on a small area dA of the sphere in the direction θ',φ' from the specimen is

$$L'(\theta',\varphi')A_{ir}\cos\theta' d\omega$$

where $d\omega$ is the elemental solid angle subtended by dA at the sample, and A_{ir} is the irradiated area of the specimen, and that leaving dA is

$$\rho_w L'(\theta',\varphi')\ A_{ir}\cos\theta' d\omega$$

Since we assume the sphere coating to be a perfect diffuser, the fraction of this flux reacing A_o, the area of the sphere viewed by the detector, is equal to the geometric view factor between areas dA and A_o, $F_{dA\rightarrow A_o}$. Thus the irradiance of A_o due to the flux incident on dA is

$$1/A\ \rho_w L'(\theta',\varphi')A_{ir}\cos\theta' d\omega \tag{34}$$

As shown by Taylor [10] and many others, the irradiance is increased by the factor $(1-\rho_w)^{-1}$ due to multiple reflections within the sphere. Thus the irradiance of A_o from the flux reflected from dA, L_{dA-A_o}, is

$$L_{A_o\ -\ dA} = \rho_w[A(1-\rho_w)]^{-1}L'(\theta',\varphi')dA_{ir}\cos\theta' d\omega \tag{35}$$

and the total irradiance $L_{A_{ir}\ -A_o}$, due to all the flux reflected from A_{ir} is

$$L_{A_{ir}\ -\ A_o} = \frac{\rho_w}{A(1-\rho_w)} A_{ir}\int_o^{2\pi} L'(\theta',\varphi')\cos\theta' d\omega \tag{36}$$

which produces a reflected radiance over the area A_o of L'_s

$$L'_s = \frac{1}{\pi}\frac{\rho_w^2}{A(1-\rho_w)} A_{ir}\int_o^{2\pi} L'(\theta',\varphi')\cos\theta' d\omega \tag{37}$$

But, by definition, the total flux reflected from the sample, F', is

$$F' = A_{ir}\int_o^{2\pi} L'(\theta',\varphi')\cos\theta' d\omega \tag{38}$$

hence L'_s is also given by

$$L'_s = \frac{1}{\pi} \frac{\rho_w^2}{A(1 - \rho_w)} F' \tag{39}$$

In order to evaluate the flux, F_o, incident on the specimen, we illuminate an area of sphere wall (the coated spherical cap in the comparison standard port) that is not shielded from A_D. The flux leaving the sphere wall is $F_o \rho_w$. The fraction of this flux reaching A_D is determined by the geometric view factor from A_{ir} to $A_D = A_D/A$. The irradiance of A_D on the first reflection is thus

$$\rho_w F_o A_D/A \cdot 1/A_D = \frac{\rho_w F_o}{A} \tag{40}$$

Again the irradiance is increased by multiple reflections, by the factor $\frac{1}{1 - \rho_w}$. Thus the total irradiance $L_{A_{ir}-A_D}$ is

$$L_{A_{ir} - A_D} = \frac{\rho_w}{A(1 - \rho_w)} F_o \tag{41}$$

and the total radiance of A_D, L'_o, will be

$$L'_o = \frac{1}{\pi} \frac{\rho_w^2}{A(1 - \rho_w)} F_o \tag{42}$$

The ratio of the radiances of A_D for the two conditions (eqs. 39 and 42) is thus

$$\frac{1}{\pi} \frac{\rho_w^2}{A(1 - \rho_w)} F' \cdot \frac{\pi A(1 - \rho_w)}{\rho_w^2 F_o} = \frac{F'}{F_o} = \rho(\theta, \varphi) \tag{43}$$

since by definition F'/F_o is the directional hemispherical reflectance, $\rho(\theta,\varphi)$ of the specimen.

Certain assumptions were made in the above derivation. First, the sphere surface was assumed to be a perfect diffuser. Second, the ratio of the total area of sphere ports to total area of the sphere was assumed to be zero. As noted previously, this ratio was about 0.0027. Third, equation (38) ignores that fraction of the reflected flux directly incident on the shield that is absorbed on the first reflection. As a rough approximation, on the order of 2% of the flux reflected by a diffusely reflecting specimen will be incident on the shield, and of this perhaps 5% will be absorbed. The total error

from this assumption is thus 0.001 of the reflected flux.

From the above, it is evident that the shield should be as small as possible, and of the highest possible reflectance. If the shield were a perfect mirror, there would be no error, since the flux would then merely be redistributed over the sphere surface, without loss.

The errors in the measurements will be analyzed in more detail in a future report.

Since the fraction of the reflected flux intercepted by the shield is greatest for a diffusely reflecting specimen, and is zero for a perfectly specular reflector, limits can be placed on the size of the error. This error will be present only in the absolute reflectance measurements. When the relative reflectance is measured for the case of a specimen and standard having identical geometric distributions of reflected flux, the losses compensate and there is no error. This will be true in measuring the reflectance of a hot specimen relative to an identical specimen at room temperature.

3.6 Modification of Auxiliary Equipment

3.6.1 Laser Source

One continuing problem in operation of the reflectometer has been fluctuation of the intensity of the laser beam. Use of a highly-regulated constant voltage power supply, and controlled variation of the input voltage, showed that the observed fluctuations were not related to variations in input voltage to the laser. The fluctuations in output when operating at the 0.6328 micron wavelength vary in amplitude from about 2 to 5 percent, and in period from about 10 minutes to an hour or more. The amplitude of the fluctuations is considerably larger at the longer wavelengths, up to as much as 50 percent in some cases.

A method was devised to correct automatically for the fluctuations in the output of the laser. The laser tube produces beams at both ends of the tube. The beam from the back of the tube is used to monitor the output, since the two beams are always proportional. The beam is chopped, attenuated and then monitored with a lead sulfide detector, and the signal amplified by a synchronous amplifier, and then mechanically rectified to produce a d.c. potential that is used as the reference potential across the slidewire of a potentiometer recorder. The beam out the front of the tube is used as the source for the reflectometer, and the signal from the detector of the reflectometer is amplified, rectified and balanced against the reference signal. In this way the recorded signal is automatically

corrected for fluctuations in power output of the laser.

The preamplifier used with the lead sulfide detector for the reference beam was designed for use with a detector with a dark resistance of 6 megohms, but the dark resistance of the cell used was only 1.6 megohms. It was necessary to modify the preamplifier by shunting the load resistor in the preamplifier to approximately equal the dark resistance of the lead sulfide detector. In addition, the d.c. power supply of the main amplifier was used to supply the bias voltage to the cell. The +240 volt power supply was connected to ground through a 100,000 ohm precision potentiometer, with a capacitor in parallel with the potentiometer to eliminate the ripple in the power supply. Thus any voltage from 0 to 240 volts could be put across the cell and load resistor. With these modifications, the preamplifier operated satisfactorily.

The entire system is now being checked for noise and linearity.

3.6.2 Heater Design

In the original design the specimen was heated by means of resistance heating elements mounted in the specimen holder. With this arrangement specimens could be heated in air to a temperature of about 1800°K. Resistance heating elements for use to higher temperatures generally require use of a non-oxidizing atmosphere surrounding the heating element, and special refractories to support the heating element and specimen. Such refractories must be not only stable at the operating temperature in the non-oxidizing atmosphere, but also non-reactive with the heating element and specimen. Materials for such an application are not readily available, particularly for use at temperatures of 2500°K or above. Induction heating eliminates many of these problems, and has been selected for heating specimens to the higher temperatures.

The induction heater should not disturb the sphere configuration, should be capable of heating the specimen to at least 2500°K (4000°F), and should not heat the sphere wall appreciably. Tests were made with an induction heater comprising a 3 in. diameter slotted copper disc concentrator, with a center hole just large enough to clear the susceptor, with the first turn of the induction coil soldered to the concentrator to provide some water cooling. A stainless steel plate with a 3 in. diameter hole was mounted above the heater, and a nickel susceptor mounted in the heater was held at 1400°K for several minutes. Only slight heating of the stainless steel was observed, and this amount of heat

could be removed easily by water cooling.

In the final design the induction coil is in the form of a flat spiral of 3/16 in. copper tubing. The first turn is silver soldered to a copper plate, 1/16 in. thick, that is shaped to the radius of the sphere. The copper plate and a bakelite ring 1/2 in. wide separating the copper plate from the stainless steel sphere form a portion of the sphere wall and are coated with barium sulfate. The susceptor is of high-purity tungsten, and is centered in the hole in the slotted copper concentrator. It is supported by a tube of stabilized zirconia. The entire heater assembly is housed in a vacuum-tight enclosure, so that measurements can be made in vacuum or inert atmosphere if desired. The portion of the stainless steel sphere wall surrounding the heater is water cooled by means of copper tubing soldered to the outside of the sphere.

3.6.3 Mirror Holder

In operation the incident laser beam must be directed alternately onto the specimen and the comparison standard. In order to avoid the necessity of realigning the mirror each time it is moved, a new mirror holder was designed and built. The mount rotates freely about an axis which is the intersection of the front surface of the mirror and the principal plane of the sphere. Adjustable stops are provided to position the mirror so that the incident beam is centered alternately on the specimen and comparison standard as the mirror contacts the two stops. The mirror is held in contact with the stop by means of magnets attached to the holder, which are attracted by the steel stops. The position of the holder about a second axis of rotation, perpendicular to the first and also in the front surface of the mirror, can be adjusted and firmly fixed by means of adjustable screws. These two adjustments permit the incident beam to be centered accurately on the specimen and comparison standard, and changed quickly from one to the other, while assuring that the beam will always return to the same preset position when the holder is in contact with one of the stops.

4. Measurements Above 2500°K (4000°F)

4.1 Background

The overall objectives of this program were to make a critical analysis of all methods of measuring emittance at temperatures in the range of 2500 to 3600°K or methods which can be extended to this temperature range. The precision, accuracy, limitations and improvements to obtain higher accuracy were to be evaluated, along with definitions of future programs, resources, and

time requirements for techniques which warrant further development in this temperature range.

4.2 Literature Survey

As a part of the study of the feasability of making direct measurements of emittance of specimens in the 2500 - 3600°K(4000 - 6000°F) temperature range, a literature survey was made in order to critically evaluate work that has been done in this temperature range. For convenience, the procedures will be classified by the method of heating the specimen.

4.2.1 Induction Heating

Clayton [11] used a rotating specimen inside an induction-heated furnace to measure emittance and transmittance of materials at high temperatures. Although the method is reported to be suitable for use at temperatures up to 2790°K (4500°F), no data are reported at temperatures above 2388°K (2800°F). The reported error in total normal emittance was 13 percent.

Pears [12] heated his specimens by induction, directly if the specimen was an electrical conductor, or by means of a tungsten or tantalum disc, 0.010 in. thick, used as a susceptor. The specimen, in the form of a disc 1/2 to 1 1/2 in. in diameter and 1/16 to 1/4 in. thick, rested on the susceptor disc. The total radiance of the hot specimen was compared to that of a blackbody cavity at the same temperature. Temperature was measured with a thermocouple at the lower temperatures, and with an optical pyrometer at temperatures above 1480°K(2500°F). The true temperature was computed from the brightness temperature measured with an optical pyrometer and the total radiance measured with a radiometer, on the basis of the graybody assumption. Errors are reported to be less than 12 percent.

Riethof and DeSantis [13] used the deep-cavity technique to measure the emittance of conducting specimens that were heated by induction. A specimen in the form of a cylinder 1/2 in. long and 1/4 in. in diameter, with a cavity .020 in. in diameter and 0.080 in. deep in the center of one face, was heated in vacuum or controlled atmosphere by induction, and the radiance from the surface of the specimen was compared to that of the cavity to obtain the emittance. Measurements were made of both total emittance and spectral emittance from 0.4 to 4.0 microns, at temperatures up to 3400°K (5660°F). No estimate of the accuracy was given.

4.2.2 Arc-Image Furnace Heating

An arc-image furnace consists of two ellipsoidal mirrors mounted on a common axis facing each other so that their second focal points coincide. An image of a carbon arc, located at the first focal point of one mirror, is formed on the specimen at the first focal point of the second mirror. The specimen is heated entirely by radiation.

Comstock [14] used an arc-image furnace to heat and irradiate a specimen for measurement of reflectance at high temperature. The incident flux, and the reflected plus the emitted flux were sampled by an ingenious light pipe that traversed the image of the source or specimen, formed at the common second focal point of both mirrors. A chopper, between the source and the scanning light pipe, interrupted the incident flux periodically so that the emitted flux could be separately evaluated. Measurements were made at temperatures up to about 4000°K (6700°F). Reproducibility was reported as ± 4 percent, but no estimate of accuracy was made.

Null and Lozier [15] used an arc-image furnace to measure the reflectance of the hot crater face of the positive electrode of an electric carbon arc, at 3800°K (6440°F). In this case a hole in the ellipsoidal mirror permitted the specimen to be viewed at an angle of 45° to the normal. Rotating choppers facilitated measurement of reflected and emitted flux separately. The precision of measurement is reported as ± 0.004 in reflectance, but no estimate of accuracy is reported.

Wilson [16] used equipment similar to that described above and used by Comstock [14], to measure the emittance and reflectance of ablation chars, carbon, graphite and zirconia to 3700°K. Errors are discussed, but are not quantitatively evaluated.

4.2.3 Solar Furnace Heating

The solar furnace is conceptually very similar to the arc-image furnace discussed above, except that the arc source is replaced by the sun, and a simple parabolic mirror is used to concentrate the solar energy on the specimen.

Blau, et. al. [17] and Laszlo, Gannon and Sheehan [18] used solar furnaces to measure reflectance of samples at very high temperatures. The basic technique was similar to that used with the arc-image furnace, except that rotating shutters, rather than a traversing light pipe, were used to facilitate measurement of incident, reflected and emitted flux. Blau et. al. reported poor results

because of instability of incoming solar flux. Laszlo et. al. apparently solved some of the problems, but reported no data.

4.2.4 Plasma Torch Heating

Cox [19] heated a disc-shaped specimen about 3/4-in. thick with a plasma torch on the front surface and a propane torch on the rear surface. The temperature of the specimen was measured at three depths below the surface, by means of an optical pyrometer sighted on the bottom of cylindrical cavities extending to the center of the specimen and thermal gradients in the specimen were computed by standard heat-transfer techniques from the measured temperatures and the observed external temperature profile of the specimen. Data are reported to 4600°F (about 2800°K). Errors are estimated to be ± 15 to 20 percent.

4.2.5 Resistance Heating

Moore, Stetson and Metcalfe [20] measured total hemispherical emittance of ceramic coatings applied to a tungsten filament that is heated by passing a current through it. The emittance is computed from the observed power input to and temperature of a short segment near the center of the specimen. Temperature is computed from the observed resistance of the tungsten wire. Data to 2800°K (4800°F) are reported for yttria-stabilized hafnia.

4.2.6 Special Techniques

There are several additional heating techniques that can be used to attain very high temperatures that apparently have not yet been applied to measurements of thermal radiation properties. These include electron beam heating, and dielectric heating. There are serious difficulties to be overcome before either of these techniques can be used for such measurements.

4.3 Discussion

None of the methods described in the literature appears to be ideally suited to measurement of the thermal radiation properties of non-metallic materials at temperatures above 2500°K (4000°F).

For direct emittance measurements, the major problem concerns temperature measurement. Non-metallic materials in general are poor thermal conductors, and somewhat translucent. Large thermal gradients will be present in the specimen unless extreme precautions are taken to assure uniform heating. Even if the specimen is heated uniformly, temperature measurement is a serious

problem, because optical and radiation pyrometers are essentially the only methods available for temperature measurement in this range, and they depend upon a knowledge of the emittance of the specimen.

For reflectance measurements the required precision of temperature measurement is much less stringent. The major problem here is to measure accurately the relatively small amount of reflected flux in the presence of the relatively large amount of emitted flux. This can be done in the case of specimens heated by radiation, as in the arc-image or solar furnace, where the incident flux is greater than the emitted flux, but the changing temperature of the specimen as the incident flux is chopped reduces the accuracy of the method. Use of a high-intensity, narrow wavelength source, such as a laser, is advantageous at the wavelengths where such sources are available.

Studies are continuing in this area to complete the critical analysis of all the ultra-high-temperature emittance measurement techniques.

An ellipsoidal mirror emissometer described below appears capable of yielding results at least as accurate as the best that can be obtained by other methods reported in the literature.

4.4 The Ellipsoidal Mirror Emissometer

4.4.1 Introduction

Essentially all radiometric procedures for measuring emittance consist of measuring the ratio of the radiance of a hot specimen to that of a blackbody radiator or other comparison standard of known emittance that is at the same temperature. Practically all of the serious problems associated with such measurements at very high temperatures are related to the generation, control and measurement of the very high temperatures.

As was mentioned in an earlier section of this report, it is even difficult to define the temperature of a specimen that is partially translucent if it is heated under conditions such that there is a thermal gradient normal to the emitting surface.

The critical requirement for temperature measurement and control is to ensure that the hot specimen and the comparison standard are at the same temperature within very close limits. The temperature of a laboratory blackbody furnace can be measured accurately with an optical pyrometer, but the brightness temperature of the specimen must be corrected for the normal spectral emittance

of the specimen in order to convert it to true temperature. The error in the measured total emittance ($\Delta\epsilon$) due to a difference in the temperatures of the specimen (T_s) and blackbody (T_b) can be expressed as follows:

$$\Delta\epsilon = \frac{4(T_s - T_b)}{T_b} \tag{44}$$

The method described in this section is based on the fact that the emittance of a test specimen depends on the ratio of two quantities, the radiance of the specimen enclosed in a blackbody cavity at the same temperature as the specimen and the radiance of the specimen enclosed in a blackbody cavity at a much lower temperature. This ratio of the radiance of the specimen under the two conditions is the emittance of the specimen, if the temperature of the specimen is the same under the two conditions. The essential condition for the specimen to appear to be in a blackbody enclosure is that the total reflected and emitted radiant flux leaving the surface be the same as that incident on the surface. This could be achieved by surrounding the specimen either with walls at its temperature, forming a true blackbody cavity, or with perfectly reflecting walls, which will form a pseudo-blackbody cavity. The latter approach is used in the instrument to be described.

4.4.2 Description of Equipment

The ellipsoidal mirror emissometer consists of five components: (1) a specimen and suitable specimen heater; (2) a self-irradiator, or an optical system for returning to the specimen the flux emitted by it, (3) a chopper or other means of intermittently blocking the emitted flux from returning to the specimen; (4) an optical system for viewing the specimen both when it is self-irradiated and when not irradiated; and (5) a suitable detector-amplifier-recorder combination to measure the flux emitted by the specimen during the periods when it is self-irradiated and not irradiated, and record the ratio of the two signals.

The detector-amplifier-recorder combination may incorporate a suitable spectrometer, if it is desired to measure spectral emittance.

One possible system incorporating the above components is shown in Figure 16. The specimen is mounted at the first focal point of an ellipsoidal mirror, and a mirror chopper is placed at the second focal point, normal to the axis of the ellipsoid. A cooled blackbody cavity behind the chopper

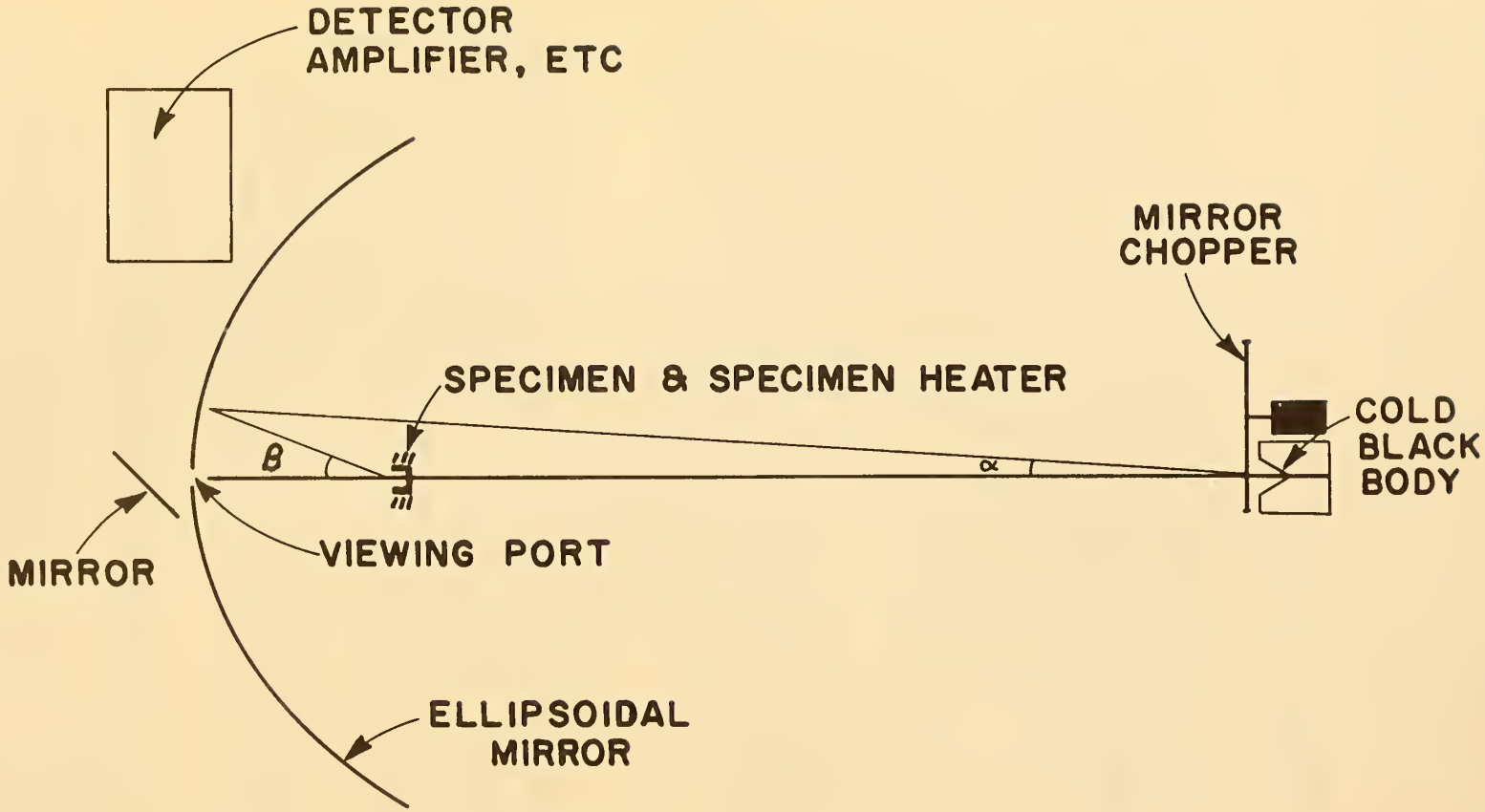

Figure 16. Schematic Diagram of Ellipsoidal Mirror Emissometer

absorbs the flux from the specimen when the chopper blade is out of the path. When the mirror chopper is in the path, nearly all of the flux emitted by the specimen is returned to it. The surface of the specimen is viewed through a small hole in the ellipsoidal mirror. The detector amplifier system measures the ratio of the radiances of the specimen when the chopper is in and out of the optical path. If there were no losses in the system, this ratio would be the normal emittance of the specimen. It is possible to correct for the losses, and thus to compute the emittance from the measured ratio.

During the period when the mirror chopper is in the optical path, most of the radiant flux leaving the specimen is returned to it, and there is very little net heat loss from the emitting surface, hence the thermal gradients normal to the emitting surface are much smaller than they would be for a freely emitting specimen at the same temperature.

4.4.3 Other Optical Systems

Several alternative optical systems could be used to return the emitted flux to the specimen. These include various combinations of paraboloidal, ellipsoidal, spherical and plane mirrors. The essential features are (1) that essentially all of the radiant flux emitted by the specimen be returned to it during a portion of a cycle, (2) that essentially none of the flux emitted by the specimen be returned to it during a portion of a cycle, and (3) that means be provided, such as a mirror or other type of chopper, to alternate between conditions (1) and (2) at a rate such that the specimen remains essentially in thermal equilibrium during an entire cycle. A chopping rate of 11 or 13 cycles per second is considered adequate to accomplish this in most cases.

It is desirable to have the fraction of the cycle during which the emitted flux is absorbed small compared to the fraction when it is reflected back to the specimen, in order to minimize the heat transfer from the specimen, and thus the thermal gradient normal to the surface.

For operation in vacuum or an inert atmosphere, it will be necessary to enclose the specimen and susceptor in a gas-tight enclosure. From several standpoints, the errors will be less if the ellipsoidal mirror and chopper are also in the enclosure, in order to avoid reflection and absorption by the enclosure.

4.4.4 Mathematical Analysis

Not all of the flux leaving the surface of the specimen will be returned to it by the optical system. The major losses are:

1) Absorption by the mirror.

2) Loss due to shading by the specimen heater and support.

3) Loss out the viewing aperture in the ellipsoidal mirror.

4) Loss due to flux scattered by the mirrors.

The losses are all related to the specific optical system used, and will be essentially independent of the specimen that is being measured, assuming that specimens are of the same dimensions. Thus it is possible to include all of these losses in a simple loss factor, which for convenience is expressed as $(1-\ell)$, where ℓ is the fraction of the flux leaving the specimen that returns to it after one passage through the system. The emitted spectral radiance of the hot specimen, $L_{\lambda s}$, will be

$$L_{\lambda, s} = \epsilon(\lambda)\, L_{\lambda, b} \tag{45}$$

where $\epsilon(\lambda)$ is the spectral emittance of the specimen at wavelength λ, and $L_{\lambda, b}$ is the spectral radiance of a blackbody radiator at the same temperature and under the same conditions. Of this emitted radiance, $\ell_\lambda \epsilon(\lambda)\, L_{\lambda b}$ will return as irradiance after one passage through the system. Of this returning irradiance, a fraction $\epsilon(\lambda)$ will be abosrbed, and the fraction $[1 - \epsilon(\lambda)]$ will be reflected, so that the reflected flux at this point will be $\ell_\lambda \epsilon(\lambda)\ [1-\epsilon(\lambda)]\, L_{\lambda, b}$. Of this the fraction ℓ_λ will again return to the surface, so that the irradiance after two passages through the system will be $\ell_\lambda^2 \epsilon(\lambda)[1-\epsilon(\lambda)]\, L_{\lambda, b}$, and of this a fraction $[1-\epsilon(\lambda)]$ will again be reflected, and so forth. Thus we get as the total radiance of the specimen, $L_{\lambda, s, t}$

$$L_{\lambda, s, t} = \epsilon(\lambda)\, L_{\lambda, b} + \ell_\lambda [1 - \epsilon(\lambda)]\ \epsilon\lambda L_{\lambda, b} + \ell_\lambda^2 [1 - \epsilon(\lambda)]^2\ \epsilon(\lambda)\, L_{\lambda, b} + \ell^3 [1 - \epsilon(\lambda)]^3$$
$$\epsilon(\lambda)\, L_{\lambda, b} + \ell^4 [1 - \epsilon(\lambda)]^4\ \epsilon(\lambda)\, L_{\lambda, b} + \cdots \tag{46}$$

This is an infinite series that reduces to

$$L_{\lambda, s, t} = \frac{\epsilon(\lambda)\, L_{\lambda b}}{1 - \ell_\lambda [1 - \epsilon(\lambda)]} \tag{47}$$

It can be seen from equation (47) that if $\ell_\lambda = 1$, or in other words, if there is no loss in the optical system,

$$L_{\lambda, s, t} = \frac{\epsilon(\lambda)\, L_{\lambda, b}}{\epsilon(\lambda)} = L_{\lambda, b} \tag{48}$$

which is the basis for the method. If the specimen is a diffuse reflector, the radiances $L_{\lambda,s,t}$ and $L_{\lambda,s}$ will be sampled by the detector through the small hole in the ellipsoidal mirror.

When the plane mirror at the second focal point of the ellipsoidal mirror is replaced by a complete absorber, none of the emitted flux is returned to the specimen, and the radiance $L_{\lambda,s}$ of the specimen then is expressed by equation (45), above.

The measured ratio of the radiances under the two conditions will be

$$\frac{L_{\lambda, s}}{L_{\lambda, s, t}} = \frac{\epsilon(\lambda)\, L_{\lambda, b}\, \{1 - \ell_\lambda [1 - \epsilon(\lambda)]\}}{\epsilon(\lambda)\, L_{\lambda, b}} = 1 - \ell_\lambda \, [1 - \epsilon(\lambda)] \tag{49}$$

If we set $L_{s,\lambda}/L_{s,\lambda,t} = R_\lambda$, we can solve for $\epsilon(\lambda)$ to get

$$\epsilon(\lambda) = \frac{R_\lambda - 1 + \ell_\lambda}{\ell_\lambda} \tag{50}$$

The uncertainty in $\epsilon(\lambda)$ can be expressed in terms of the uncertainties in R_λ and ℓ_λ as

$$\Delta\epsilon(\lambda) = \frac{\Delta R_\lambda}{\ell_\lambda} + \frac{(1 - R_\lambda)\, \Delta \ell_\lambda}{\ell_\lambda^2 + \ell_\lambda \Delta \ell_\lambda} \tag{51}$$

Assuming $\epsilon(\lambda) = 0.50$, $R_\lambda = 0.60$, and $\ell_\lambda = 0.80$, the error in $\epsilon(\lambda)$ due to an uncertainty of 0.01 in R_λ and 0.01 in ℓ_λ will give an uncertainty of $\epsilon(\lambda)$ of less than 0.02, or 4%. Precision of this order should be attainable with careful work.

The above analysis was based on the use of radiances, L. Radiance is defined as flux, Φ, per unit area of surface, A, projected normal to the direction of propagation, and per unit solid angle, ω. Hence radiance, L, is defined as

$$L = d^2 \Phi / (\cos \theta \, dA \, d\omega) \tag{52}$$

where θ is the angle between the direction of propagation and the normal to the emitting surface.

To make equations (45–49) rigorously correct, each radiance, L, should contain an area factor A, and a solid angle factor, ω.

$$\Phi = \int_A \int_\omega L \cos\theta \, d\omega \, dA \tag{53}$$

All of the equations (45–49) have been simplified by omitting the integral factors.

A more rigorous analysis of the system shows that there will be a contribution to the total radiance of the specimen from the flux emitted by the specimen and susceptor and reflected directly back to the specimen by the ellipsoidal mirror. This requires modification of equations (45) and (47).

The diffuse configuration factor from the specimen to its image reflected in the ellipsoidal mirror is defined as f_1 and that from the susceptor to the image of the specimen is defined as f_2. A_s is the area of the specimen, and A_u is the area of the susceptor. ω_v is the solid angle of flux received by the detector. The specimen is assumed to be a diffuse emitter and reflector. The susceptor is assumed to be a diffuse emitter, but a specular reflector. The radiance of the susceptor is defined as L_u.

When the mirror chopper is out of the path and is not reflecting flux back to the specimen, the radiance of the specimen will consist of the emitted flux, $\epsilon(\lambda) L_{\lambda, b,}$ plus the flux emitted by the susceptor and reflected directly back to the specimen. Since the susceptor is a specular reflector, flux from the susceptor and specimen reflected back to the susceptor will be reflected out of the optical path and lost. Since the specimen is a diffuse reflector, there will be multiple reflection between the specimen and ellipsoidal mirror. To simplify the derivation, we will consider separately the flux originating from the specimen and susceptor. The flux reaching the detector that was emitted by the specimen is $L_{s,\lambda} A_s \omega_v$ (specimen). After one reflection from the ellipsoidal mirror it is

$$L_{s,\lambda} A_s \omega_v \text{ (spec.)} = \epsilon(\lambda)\, L_{b,\lambda}\, A_s\, \omega_v + \epsilon(\lambda)\, L_{b,\lambda} A_s\, \omega_v\, f_1 \rho_1 [1 - \epsilon(\lambda)]$$

and after multiple reflections reduces to

$$L_{s,\lambda}\ A_s\ \omega_v\ \text{(spec.)} = \frac{\epsilon(\lambda) L_{b,\lambda} A_s\ \omega_v}{1 - f_1\, \rho_1\, [1 - \epsilon(\lambda)]} \tag{54}$$

The flux reaching the detector that was emitted by the susceptor is $L_s A_s \omega_v$ (susceptor). After the first reflection from the ellipsoidal mirror it is

$$L_{s,\lambda} A_s \omega_v \text{ (susceptor)} = A_U L_U f_2 \rho_1 \omega_v [1 - \epsilon(\lambda)] + A_U L_U f_2 f_1 \rho_1^2 \omega_v [1 - \epsilon(\lambda)]^2$$

and after multiple reflections reduces to

$$L_{s,\lambda} A_s \omega_v \text{ (susceptor)} = \frac{A_U L_U f_2 \rho_1 \omega_v [1 - \epsilon(\lambda)]}{1 - f_1 \rho_1 [1 - \epsilon(\lambda)]} \tag{55}$$

Combining equations (54) and (55)

$$L_{s,\lambda} A_s \omega_v = \frac{\epsilon(\lambda) L_{b,\lambda} A_s \omega_v + A_U L_U f_2 \rho_1 \omega_v [1 - \epsilon(\lambda)]}{1 - f_1 \rho_1 [1 - \epsilon(\lambda)]} \tag{56}$$

or

$$A_s L_{s,\lambda} = \frac{\epsilon(\lambda) L_{b,\lambda} A_s + A_U L_U f_2 \rho_1 [1 - \epsilon(\lambda)]}{1 - f_1 \rho_1 [1 - \epsilon(\lambda)]} \tag{57}$$

When the mirror chopper is in the optical path, a fraction, ℓ_λ, of the flux leaving the specimen, which will be $L_{s,\lambda} A_s \pi$, will be returned to the specimen, and of this a fraction $[1 - \epsilon(\lambda)]$ will be diffusely reflected into the hemisphere, and a fraction ω_v / π of the reflected flux will reach the detector. Hence after one reflection, we can write for the flux emitted by the specimen

$$L_{s,\lambda,t} A_s \omega_v \text{ (spec.)} = \epsilon(\lambda) L_{b,\lambda} A_s \omega_v + \epsilon(\lambda) L_{b,\lambda} A_s \pi \omega_v / \pi \{f_1 \rho_1 [1 - \epsilon(\lambda)] + \ell_\lambda [1 - \epsilon(\lambda)]\}$$

and after multiple reflections this reduces to

$$L_{s,\lambda,t} A_s \omega_v \text{ (spec.)} = \frac{\epsilon(\lambda) L_{b,\lambda} A_s \omega_v}{1 - (f_1 \rho_1 + \ell_\lambda)[1 - \epsilon(\lambda)]} \tag{58}$$

Similarly, the contribution from the flux emitted by the susceptor will be

$$L_{s,\lambda,t} A_s \omega_v \text{ (susceptor)} = \frac{f_2 L_U A_U \rho_1 [1 - \epsilon(\lambda)] \omega_v}{1 - (f_1 \rho_1 + \ell_\lambda)[1 - \epsilon(\lambda)]} \tag{59}$$

Combining equations (58) and (59) we get,

$$L_{s,\lambda,t} A_s \omega_v = \frac{\epsilon(\lambda) L_{b,\lambda} A_s \omega_v + f_2 L_U A_U \rho_1 [1 - \epsilon(\lambda)] \omega_v}{1 - (f_1 \rho_1 + \ell_\lambda)[1 - \epsilon(\lambda)]} \tag{60}$$

and the measured ratio, R_λ, becomes

$$R_\lambda = \frac{L_{s,\lambda} A_s \omega_v}{L_{s,\lambda,t} A_s \omega_v} = \frac{1 - (f_1 \rho_1 + \ell_\lambda)[1 - \epsilon(\lambda)]}{1 - f_1 \rho_1 [1 - \epsilon(\lambda)]} \tag{61}$$

Solving for $\epsilon(\lambda)$

$$\epsilon(\lambda) = \frac{\ell_\lambda - (1 - f_1 \rho_1)(1 - R_\lambda)}{\ell_\lambda - f_1 \rho_1 (R_\lambda - 1)} \tag{62}$$

It should be noted in equation (62) that only ρ_1, f_1 and ℓ_λ need be evaluated.

4.4.5 Evaluation of System Parameters

Reasonably good values of the parameters ρ_1, f_1 and ℓ_λ may be computed if the geometry of the system and the reflectances of the ellipsoidal and plane mirrors are known. For the system under consideration, the following geometry for the system will be assumed.

Focal length of the ellipsoid = 2c = 17 in.

Latus rectum = S = 6.166 in.

Eccentricity = e = 0.70103

Semi-major axis = a = 12.125 in.

Heater coil radius = h_1 = 1.00 in.

Susceptor radius = h_2 = 0.50 in.

Viewing port radius = 0.18 in., centered on the major axis of the ellipse.

Spectral reflectance of ellipsoidal mirror = $\rho_1(\lambda)$ = 0.97.

Spectral reflectance of plane mirror = $\rho_2(\lambda)$ = 0.97

In addition, two angles will be defined as follows. β is the angle of a beam of radiation from the normal to the specimen at the first focal point, and α is the angle of a beam of radiation from the normal to the plane mirror at the second focal point.

The above geometrical characteristics of the system were selected for the analysis because they can be readily achieved without excessive cost. Improved operation can be achieved by selection of more favorable geometry, but the above will suffice for this preliminary analysis.

The flux losses, represented by $(1 - \ell_\lambda)$, must include the flux lost out the viewing port, plus the flux absorbed by the mirrors and that blocked by the specimen heater and supports.

The fraction δ_1 of the flux leaving the specimen at the first focal point that is blocked by the heater, susceptor and specimen, from returning to the specimen from the plane mirror at the second focal point, is given by

$$\delta_1 = \frac{1}{\pi} \int_0^{\beta_1} \cos \beta \, d\omega = \sin^2 \beta_1 \qquad (63)$$

β_1 is defined as the angle to the major axis of the ellipsoid at which a ray leaves the first focal point of the ellipsoid to just graze the edge of the heater when reflected by the ellipsoidal mirror. The angle α_1 is the angle to the major axis of the ellipsoid at the second focal point, and can be computed as

$$\tan \alpha_1 = h_1 / 2c \qquad (64)$$

β and α for any ray are related by

$$\sin \beta = \frac{(1 - e^2) \sin \alpha}{(1 - e^2 - 2e \cos \alpha)} \qquad (65)$$

The hole loss and the flux blocked by the support can be computed in a similar manner. In the ellipsoid described here, the hole loss is included in the shading loss, but is included to indicate its magnitude. The various parameters have been computed to be

$\delta_1 = 0.106$ = fraction blocked by specimen, susceptor and heater.

$\delta_2 = 0.015$ = fraction blocked by supports.

$\delta_3 = 0.0025$ = fraction passing out the viewing port in the ellipsoidal mirror.

$\delta_4 = 0.007$ = fraction returned to specimen directly by ellipsoidal mirror = f_1 in equations (54-62).

$\delta_5 = 0.025$ = fraction going to the susceptor.

The value of δ_4 is low because the viewing port is located in the area of the mirror that would normally reflect flux back to the specimen. For a mirror in which the viewing port is outside of this area, the value would be increased by the amount of δ_3. The view factor f_2 in equations (54-62) can be computed from δ_5 and the areas of the susceptor, A_U, and specimen, A_S, as

$$f_2 = \delta_5 A_S / A_U \qquad (66)$$

We can compute ℓ_λ from the above parameters as

$$\ell_\lambda = (1 - \delta_1 - \delta_2) \rho_1^2 \rho_2 \qquad (67)$$

Substituting the given values in equation (67), $\ell_\lambda = (1 - 0.106 - 0.015)\, 0.97^3 = 0.802$. Thus all of the system parameters required for solution of equation (62) have been obtained. Construction of

an ellipsoidal mirror emissometer will be financed on NBS funds.

5. Summary

The shallow-cavity technique for measuring emittance was found to be subject to unacceptably large errors in measurements made on partially translucent specimens of nonmetallic materials, and especially on ceramic oxide materials. The translucency error was found to be as large as +60%, and the error due to thermal gradients in the specimen was found to be on the order of -10%. Two new techniques that show promise of greatly reducing these errors were developed, and preliminary tests indicate that the translucency error is largely eliminated. Corrections can be made for the temperature difference error, if the magnitude of the thermal gradients is known. Considerable progress was made in developing computer codes to evaluate the thermal gradients from the thermal conductivity and emittance of the specimen.

The laser-source integrating sphere reflectometer, as originally designed, was found to give reflectance data at 0.6328 micron that was in error by about ± 0.02 in reflectance. This was as much as a 20 percent error for specimens of low reflectance. The integrating sphere and associated equipment has been redesigned to improve accuracy and precision. Final evaluation awaits completion of the modifications.

A survey of the literature on techniques for measuring thermal radiation properties of solids in the 4000-6000°F (2500° to 3600°K) temperature range indicates that measurements to an accuracy of better than 10 to 20 percent are very difficult to make. A newly-designed ellipsoidal mirror emissometer shows promise of giving accuracies at least as good as those available by the best alternative technique.

6. References

[1] Gouffe, A., "Temperature Corrections of Artificial Blackbodies, Taking Multiple Internal Diffusion into Consideration." NRL Trans. 429, translated from Revue d'Opt. 24 1 - 10 (1945).

[2] Kelly, F. J. and Moore, D. G., "A Test of Analytical Expressions for the Thermal Emissivity of Shallow Cylindrical Cavities." Applied Optics 4 31 (1965).

[3] Moore, D. G., "Investigation of Shallow Reference Cavities for High-Temperature Emittance Measurements." Measurement of Thermal Radiation Properties of Solids, J. C. Richmond, Ed., NASA SP 31 pp 515-525. (1963).

[4] Clark, H. E., and Moore, D. G., "Method and Equipment for Measuring Thermal Emittance of Ceramic Oxides from 1200° to 1800°K." Symposium on Thermal Radiation of Solids, S. Katzoff, Ed. NASA SP 55, ML-TDR 64-159, pp 241, 257 (1965).

[5] McCracken, D. D., and Dorn, W. S., Numerical Analysis and Fortran Programming.

[6] Olson, O. H., and Morris, J. C., "Determination of Emissivity and Reflectivity Data on Aircraft Structural Materials," WADC TR 56-222, Part 3, 1959.

[7] Pears, C. D., "The Thermal Properties of Twenty Six Solid Materials to 5000°F or Their Destruction Temperatures." ASD-TR 62-765 Jan. 1963.

[8] Cox, R. C., "Emittance of Zirconia to 4600°F." Chance-Vought Corp. Report 3/14000/2R19 April 1962.

[9] McNicholas, H. J., "Absolute Methods in Reflectometry." NBS Jour. Res. 1 29-73 (1928).

[10] Taylor, A. H., "Measurement of Diffuse Reflection Factors and a New Absolute Reflectometer." Scientific Papers of NBS 16 421-436 (1920).

[11] Clayton, W. A., "A 500°F to 4500°F Thermal Radiation Test Facility for Transparent Materials." Measurement of Thermal Radiation Properties of Solids, NASA Special Publication SP-31, pp 445-460.

[12] Pears, C. D., "Some Problems in Emittance Measurements at the Higher Temperatures and Surface Characterization." Measurement of Thermal Radiation Properties of Solids, NASA Special Publication SP-31, pp 541-551.

[13] Riethof, T. R., and DeSantis, V. J., "Techniques of Measuring Normal Spectral Emissivity of Conductive Refractory Compounds at High Temperatures." Measurement of Thermal Radiation Properties of Solids, NASA Special Publication SP-31, pp 565-583. (1963).

[14] Comstock, D. F., Jr., "A Radiation Technique for Determining the Emittance of Refractory Oxides." Measurement of Thermal Radiation Properties of Solids, NASA SP-31, pp 461-468. (1963).

[15] Null, M. R., and Lozier, W. W., "Measurement of Reflectance and Emittance at High Temperatures with a Carbon Arc - Image Furnace." Measurement of Thermal Radiation Properties of Solids, NASA SP-31, pp 535-539 (1963).

[16] Wilson, R. G., "Hemispherical Spectral Emittance of Ablation Chars, Carbon and Zirconia (to 3700°K)." Symposium on Thermal Radiations of Solids, NASA SP 55, pp 259-275. (1965).

[17] Blau, H. H., Jr. et. al., "High Temperature Thermal Radiation Properties of Solid Materials." Air Force Report AF CRC TN-60-146, October, 1960.

[18] Lazlo, T. S., Gannon, R. E., and Sheehan, P. J., "Emittance Measurements of Solids Above 2000°C." Symposium on Thermal Radiation of Solids, NASA SP-55, pp 277-286. (1965).

[19] Cox, R. L., "A Technique for Measuring Thermal Radiation Properties of Translucent Materials at High Temperature." Measurement of Thermal Radiation Properties of Solids, NASA SP 31, pp 469-481. (1963).

[20] Moore, V. S., Stetson, A. R. and Metcalfe. A. G., "Emittance Measurements of Refractory Oxide Coatings up to 2900°K." Measurements of Thermal Radiation Properties of Solids, NASA SP 31, pp 527-533. (1963).

[21] Birkhoff, G. and MacLane, S., A Survey of Modern Algebra. p 216.

[22] Walsh, J. W. T., Proc. Phys. Soc. (London) 32, 59 (1920).

7. Appendix I. Computation of Thermal Gradients

7.1 Interreflection Algebra

There are three basic types of relations that must be expressed. They are in the following equations.

$$B(\underset{\sim}{x}) = \rho(\underset{\sim}{x})\, H(\underset{\sim}{x}) \tag{a1}$$

$$Q_\alpha = \int_c H(\underset{\sim}{x})\, \alpha(\underset{\sim}{x})\, dA(\underset{\sim}{x}) \tag{a2}$$

$$H(\underset{\sim}{x}) = \int_c B(\underset{\sim}{x})\, K(\underset{\sim}{x}_o, \underset{\sim}{x})\, dA(\underset{\sim}{x}_o) \tag{a3}$$

where $B(\underset{\sim}{x})$ is the flux per unit area leaving an element of area $dA(\underset{\sim}{x})$ located at $\underset{\sim}{x}$, $\rho(\underset{\sim}{x})$ is the reflectance of the surface at $\underset{\sim}{x}$, $H(\underset{\sim}{x})$ is the flux per unit area incident on the surface at $\underset{\sim}{x}$, Q_α is the amount of flux absorbed in a cavity when the incident flux per unit area $H(\underset{\sim}{x})$ falls on each point $\underset{\sim}{x}$, and $\int_c$ indicates the integral over the cavity. $K(\underset{\sim}{x}_o, \underset{\sim}{x})$ is the diffuse angle factor or "geometric factor" between an element of area $dA(\underset{\sim}{x}_o)$ from which flux is diffusely radiating and the element of area $dA(\underset{\sim}{x})$ which receives the flux.

Each one of the functions $H(\underset{\sim}{x})$, $\rho(\underset{\sim}{x})$, $B(\underset{\sim}{x})$, and $\alpha(\underset{\sim}{x})$ can be thought of as vectors in an infinite dimensional vector space, and each can be expressed in terms of some complete set of basis functions (basis vectors) in that space. Since this functional vector space has an infinite number of dimensions, an infinite number of basis vectors are required to span the space. Thus, a given function may require an infinite number of component basis functions for its expression. Obviously no one can do a practical calculation with an infinite number of components for each vector, so it has been customary to reduce the number of dimensions of the space to some finite number N when any practical calculation is done. This is a familiar procedure in physics and engineering. For example, if one wants to express a complex periodic function in terms of its Fourier components, one, in general, must use an infinite number of components. If, however, one has some practical calculation to do, it is necessary to stop with some finite number of components.

An interreflection calculation is very similar. Strictly speaking, equations (a1), (a2), and (a3) are statements about each one of the infinite number or mathematical points on a cavity surface, but, to get practical results, it is customary to express the infinitely fine-grained information in the function B(x) in terms of a coarse-grained N dimensional vector $\underset{\sim}{B}$, and instead of considering the

infinitesimal surface element $dA(\underset{\sim}{x})$, we consider a number of finite surface areas ΔA arranged in vector form $\underset{\sim}{\Delta A}$. It is the same with $H(\underset{\sim}{x})$, $\rho(\underset{\sim}{x})$, $\alpha(\underset{\sim}{x})$, or any function of $\underset{\sim}{x}$.

$$H(\underset{\sim}{x}) \rightarrow \begin{matrix} H_1 \\ H_2 \\ \cdot \\ \cdot \\ H_N \end{matrix} = \underset{\sim}{H} \qquad B(\underset{\sim}{x}) \rightarrow \begin{matrix} B_1 \\ B_2 \\ \cdot \\ \cdot \\ B_N \end{matrix} = \underset{\sim}{B} \qquad dA(\underset{\sim}{x}) \rightarrow \begin{matrix} \Delta A_1 \\ \Delta A_2 \\ \cdot \\ \cdot \\ \Delta A_N \end{matrix} = \underset{\sim}{\Delta A} \tag{a4}$$

In the following we will denote the N-dimensional column vector corresponding to any function $w(\underset{\sim}{x})$ by the vector symbol $\underset{\sim}{w}$. The component w_i is an average value of the function $w(\underset{\sim}{x})$ on the area ΔA_i ; mathematically it is just

$$w_i = \int_{\Delta A_i} \frac{w(\underset{\sim}{x})\, dA(\underset{\sim}{x})}{\Delta A_i} \tag{a5}$$

With these kinds of vectors in the vector space, it is desired that the theory be a complete analogue of the functional theory. Thus equations (a1), (a2) and (a3) must be expressible in a vector form. In order to do this, it will be very helpful if we first consider the set of basis vectors that will be used.

The most convenient set of N basis vectors $\left\{ \underset{\sim}{\eta}_i \right\}_{i=1}^{i=N}$ is the one which gives us $B = \Sigma_i B_i \underset{\sim}{\eta}_i$. Then the basis vectors have the ordinary representation

$$\underset{\sim}{\eta}_1 = \begin{matrix} 1 \\ 0 \\ \cdot \\ \cdot \\ 0 \end{matrix} \qquad \underset{\sim}{\eta}_2 = \begin{matrix} 0 \\ 1 \\ \cdot \\ \cdot \\ 0 \end{matrix} \qquad \underset{\sim}{\eta}_N = \begin{matrix} 0 \\ 0 \\ \cdot \\ \cdot \\ 1 \end{matrix} \tag{a6}$$

and the vector $\underset{\sim}{B}$ has (for example) the following form.

$$\underset{\sim}{B} = \begin{matrix} B_1 \\ B_2 \\ \cdot \\ \cdot \\ B_N \end{matrix} \tag{a7}$$

The vector space analogy of Equation (a1) is

$$\underset{\sim}{B} = \underset{\sim}{\rho}\, \underset{\sim}{H} \tag{a8}$$

$$\Sigma_i \; B_i \underset{\sim}{\eta}_i = \Sigma_i (\rho_i \underset{\sim}{\eta}_i) \; \Sigma_j (H_j \underset{\sim}{\eta}_j) = {}_{i}\Sigma_{j} \; \rho_i \; H_j \; \underset{\sim}{\eta}_i \; \underset{\sim}{\eta}_j \tag{a9}$$

In the above equations a vector valued multiplication operates in the vector space. This type of vector multiplication must be commutative, distributive and associative, because it must be the analog of the ordinary multiplication of functions. In addition the multiplication operation must be linear in the sense that if a and b are any real numbers and if $\underset{\sim}{u}$, $\underset{\sim}{v}$, and $\underset{\sim}{w}$ are any vectors,

then $$\underset{\sim}{u}\,(a\underset{\sim}{v} + b\underset{\sim}{w}) = a\,(\underset{\sim}{u}\,\underset{\sim}{v}) + b\,(\underset{\sim}{u}\underset{\sim}{w}) \tag{a10}$$

and $$(a\underset{\sim}{v} + b\underset{\sim}{w})\,\underset{\sim}{u} = a\,(\underset{\sim}{v}\underset{\sim}{u}) + b\,(\underset{\sim}{w}\underset{\sim}{u}) \tag{a11}$$

A vector space having a vector valued multiplication operation which is linear, associative, and distributive is known as a linear algebra.

A linear multiplication operation in a vector space can be specified by giving the rule for the multiplication of the set of basis vectors amongst each other; that is

$$\underset{\sim}{x}\underset{\sim}{y} = \sum_{i,j} x_i \underset{\sim}{\eta}_i\, y_j \underset{\sim}{\eta}_j = \sum_{i,j} x_i\, y_i \underset{\sim}{\eta}_i \underset{\sim}{\eta}_j \tag{a12}$$

and if all the vectors $\underset{\sim}{\eta}_i \underset{\sim}{\eta}_j$ are known then the multiplication operation is completely specified. In the case which we have under discussion the multiplication table for the basis vectors is quite simple (Table 1). The rule is

$$\underset{\sim}{\eta}_i\, \underset{\sim}{\eta}_j = \delta_{ij}\underset{\sim}{\eta}_i \tag{a13}$$

where δ_{ij} is the Kronecker delta

$$\begin{aligned} \delta_{ij} &= 1 \text{ if and only if } i = j \\ &= 0 \text{ if and only if } i \neq j. \end{aligned} \tag{a14}$$

Table 1.

	0	$\underset{\sim}{\eta}_1$	$\underset{\sim}{\eta}_2$	$\underset{\sim}{\eta}_3$	. . .
0	0	0	0	0	
$\underset{\sim}{\eta}_1$	0	$\underset{\sim}{\eta}_1$	0	0	
$\underset{\sim}{\eta}_2$	0	0	$\underset{\sim}{\eta}_2$	0	
$\underset{\sim}{\eta}_3$	0	0	0	$\underset{\sim}{\eta}_3$	
.					
.					
.					

Also there exists a vector $\underset{\sim}{1}$ analgous to the scalar 1 such that for any vector $\underset{\sim}{w}$

$$\underset{\sim}{1}\,\underset{\sim}{w} = \underset{\sim}{w}\,\underset{\sim}{1} = \underset{\sim}{w} \tag{a15}$$

Written out longhand the vector $\underset{\sim}{1}$ is

$$\begin{matrix} 1 \\ 1 \\ 1 \\ \cdot \\ \cdot \\ 1 \end{matrix} \qquad \text{(a16)}$$

For every vector $\underset{\sim}{w}$ such that none of the components of $\underset{\sim}{w}$ is equal to zero, there exists a vector $\underset{\sim}{w}^{-1}$ such that $\underset{\sim}{w}\,\underset{\sim}{w}^{-1} = \underset{\sim}{1}$. The vector $\underset{\sim}{w}^{-1}$ can be easily constructed when $\underset{\sim}{w}$ is known. If $\underset{\sim}{w} = \Sigma_i\, w_i\, \underset{\sim}{\eta}_i$, then $w^{-1} = \Sigma_i\, (1/w_i)\, \underset{\sim}{\eta}_i$. It is easy to see that if any w_i is equal to zero, no finite inverse vector for $\underset{\sim}{w}$ exists, since the magnitude of one of the components of $\underset{\sim}{w}^{-1}$ would be 1/0.

One of the more important theorems that one can prove about a linear algebra is that for each N-dimensional linear algebra there exists an isomorphic set of N x N linear transformations (matrices) such that the operations of vector addition and multiplication and also multiplication by a scalar (real number) are preserved under the isomorphism [21]. (An isomorphism is a one-to-one correspondence between two sets such that the structure of certain operations in those sets is preserved).

It is not difficult at all to find the set of matrices which is isomorphic to the set of vectors under consideration.

The vector equation (in long form) is:

$$\begin{matrix} \rho_1 H_1 \\ \rho_2 H_2 \\ \cdot \\ \cdot \\ \cdot \\ \rho_N H_N \end{matrix} \quad = \quad \begin{matrix} \rho_1 & H_1 \\ \rho_2 & H_2 \\ \cdot & \cdot \\ \cdot & \cdot \\ \cdot & \cdot \\ \rho_N & H_N \end{matrix} \qquad \text{(a17)}$$

This can be represented equally well by a product of diagonal matrices.

$$\begin{matrix} \rho_1 H_1 & 0 & \cdot & \cdot & 0 \\ 0 & \rho_2 H_2 & & & \cdot \\ \cdot & & \cdot & & \cdot \\ \cdot & & & \cdot & 0 \\ 0 & \cdot & \cdot & 0 & \rho_N H_N \end{matrix} \quad = \quad \begin{matrix} \rho_1 & 0 & \cdot & \cdot & 0 \\ 0 & \rho_2 & & & \cdot \\ \cdot & & \cdot & & \cdot \\ \cdot & & & \cdot & 0 \\ 0 & \cdot & \cdot & 0 & \rho_N \end{matrix} \quad \begin{matrix} H_1 & 0 & \cdot & \cdot & 0 \\ 0 & H_2 & & & \cdot \\ \cdot & & \cdot & & \cdot \\ \cdot & & & \cdot & 0 \\ 0 & \cdot & \cdot & 0 & H_N \end{matrix} \qquad \text{(a18)}$$

It is easy to see that the matrix multiplication in equation (a8) does essentially the same thing with the i^{th} diagonal elements of the matrices as the vector multiplication in equation (a7) does with the i^{th} components of the vectors. One can see intuitively that an isomorphism exists and the proof of this is

quite easy also.

It is easy to show that vector addition and sealar multiplieation are preserved under this isomorphism. We ean denote the isomorphism by τ and its inverse τ^{-1} sueh that

$$\tau \begin{matrix} w_1 \\ w_2 \\ . \\ . \\ w_N \end{matrix} = \begin{matrix} w_1 & 0 & & 0 \\ 0 & w_2 & & . \\ . & & . & . \\ . & & . & 0 \\ 0 & & & w_N \end{matrix} \tag{a19}$$

and

$$\tau^{-1} \begin{matrix} w_1 & 0 & . & . & 0 \\ 0 & w_2 & & & . \\ . & & . & & . \\ . & & & . & . \\ 0 & . & . & . & w_N \end{matrix} = \begin{matrix} w_1 \\ w_2 \\ . \\ . \\ w_N \end{matrix} \tag{a20}$$

If we denote veetor by a veetor symbol $\underset{\sim}{w}$, then we ean denote the diagonal matrix which corresponds to $\underset{\sim}{w}$ by $\tau(\underset{\sim}{w})$; however, the notation would be somewhat simplified if one simply denoted the operator by removing the veetor symbol, for example

$$\tau(\underset{\sim}{w}) = w. \tag{a21}$$

It is a useful property of these diagonal matrices that the operation of one, say $\underset{\sim}{w}$, by ordinary matrix multiplieation on a veetor $\underset{\sim}{v}$ gives the same result as the multiplieation of the original veetor $\underset{\sim}{w}$ on the veetor $\underset{\sim}{v}$, i.e. for any vectors $\underset{\sim}{v}$, $\underset{\sim}{w}$

$$\underset{\sim}{w}\underset{\sim}{v} = w\underset{\sim}{v} = \tau(\underset{\sim}{w})\underset{\sim}{v} \tag{a22}$$

The next operation for which we wish to find an analogue is shown in equation (a2). In this equation two funetions $\underset{\sim}{H}(\underset{\sim}{x})$ and $\underset{\sim}{\alpha}(\underset{\sim}{x})$, (or three funetions if we consider $d\underset{\sim}{A}(\underset{\sim}{x})$ as a function) are operated on so as to give a scalar (single number) result Q_α.

In veetor space language this is denoted by $[\underset{\sim}{A}, \underset{\sim}{B}, \underset{\sim}{C}]$.

$$Q_\alpha = [\underset{\sim}{\alpha}, \underset{\sim}{H}, \underset{\sim}{\Delta A}] \tag{a23}$$

This is ealled a trilinear form beeause it maps three vectors, $\underset{\sim}{\alpha}$, $\underset{\sim}{H}$, and $\underset{\sim}{\Delta A}$, into a scalar Q_α in a linear fashion, i.e., linear in the sense that for any sealars γ, λ, and veetors $\underset{\sim}{w}$, $\underset{\sim}{x}$, $\underset{\sim}{y}$, and $\underset{\sim}{z}$,

$$\begin{aligned} [\gamma\underset{\sim}{w} + \lambda\underset{\sim}{x}, \underset{\sim}{y}, \underset{\sim}{z}] &= \gamma[\underset{\sim}{w}, \underset{\sim}{y}, \underset{\sim}{z}] + \lambda[\underset{\sim}{x}, \underset{\sim}{y}, \underset{\sim}{z}] \\ [\underset{\sim}{w}, \gamma\underset{\sim}{x} + \lambda\underset{\sim}{y}, z] &= \gamma[\underset{\sim}{w}, \underset{\sim}{x}, \underset{\sim}{z}] + \lambda[\underset{\sim}{w}, \underset{\sim}{y}, \underset{\sim}{z}] \\ [\underset{\sim}{w}, \underset{\sim}{x}, \gamma\underset{\sim}{y} + \lambda\underset{\sim}{z}] &= \gamma[w, x, z] + \lambda[\underset{\sim}{w}, \underset{\sim}{x}, \underset{\sim}{z}] \end{aligned} \tag{a24}$$

In addition the trilinear form that is considered here has the special property that it is equivalent to a bilinear form on two vectors, one of which is the vector product of the other two.

$$Q_\alpha = [\underset{\sim}{\alpha}, \underset{\sim}{H}\underset{\sim}{\Delta A}] \tag{a25}$$

Also it can be considered as a linear functional of the one triple product vector

$$Q_\alpha = [\underset{\sim}{\alpha}\underset{\sim}{H}\underset{\sim}{\Delta A}] \tag{a26}$$

This final operation--the linear functional shown in equation (a26) -- is perhaps the most useful and most easily understood operation. Q_α is just the sum of all of the components of the vector $(\underset{\sim}{\alpha}\underset{\sim}{H}\underset{\sim}{\Delta A})$.

The set of all possible linear functionals on a vector space constitutes a vector space, which is closely related to the original vector space. The vector space of linear functionals is known as the dual space of the original vector space, and each vector in the original vector space has a conjugate vector (or linear functional) in the dual space. In quantum mechanics this is symbolized by the famous bra or ket notation of Dirac. A bra is the symbol $<|$, and a ket is the symbol $|>$. A ket stands for a vector; and if the vector has a name, say $\underset{\sim}{\alpha}$, then the ket is written as $|\alpha>$. Similarly a bra stands for a linear functional or a vector in the dual space to the original vector space. The vector isomorphic to the ket $|\alpha>$ is the bra $<\alpha|$. Since the scalar field onto which these linear functionals map the vectors is the field of real numbers, we do not have to worry about the complications that ordinarily arise in quantum mechanics because a complex scalar field is used. In order to construct the basis of the dual space, one constructs the set of linear functionals $\left\{<\gamma_i|\right\}_{i=1}^{i=N}$ which are such that any one of these operating on its conjugate basis vector $|\eta_j>$ gives the value 1 and operating on any other basis vector gives the value 0. Thus the set of basis vectors $\left\{<\gamma_i|\right\}$ in the dual space is constructed such that

$$<\gamma_i|\eta_j> = \delta_{ij} \tag{a27}$$

where δ_{ij} is the Kronecker delta function. In terms of these operators then we have

$$Q_\alpha = <1 \mid \alpha H \Delta A> = (\Sigma_i <\gamma_i| \,)\ (\Sigma_j\ \alpha_j\ H_j\ \Delta A_j \mid \eta_j>) \tag{a28}$$

$$= {}_{i,j}\Sigma \alpha_i H_i \Delta A_j <\gamma_i \mid \eta_j>\ {}_{i,j}\Sigma\ \alpha_i\ H_i\ \Delta A_j \delta_{ij} = \Sigma_j\ \alpha_j\ H_j\ \Delta A_j$$

In terms of the operators corresponding to the vectors, this equation is

$$Q_\alpha = <1 \mid \alpha H \Delta A \mid 1> \tag{a29}$$

since α, H and dA are symmetric (Hermetian) operators

$$Q_\alpha = \langle \alpha \mid H \mid \Delta A \rangle \tag{a30}$$

A second way of expressing equation (a2) is completely in terms of the operators α, H and dA and the trace operation.

$$Q_\alpha = \text{trace } (\alpha H \Delta A) \tag{a31}$$

where the trace of a matrix is the sum of its diagonal terms, for example

$$\text{trace } M = \text{trace} \begin{matrix} M_{11} & M_{12} & M_{13} \\ M_{21} & M_{22} & M_{23} \\ M_{31} & M_{32} & M_{33} \end{matrix} = M_{11} + M_{22} + M_{33} \tag{a32}$$

thus

$$Q_\alpha = \begin{matrix} \alpha_1 H_1 \Delta A_1 & 0 & . & . & 0 \\ 0 & \alpha_2 H_2 \Delta A_2 & . & . & . \\ . & . & . & . & . \\ . & . & . & . & 0 \\ 0 & . & . & 0 & \alpha_N H_N \Delta A_N \end{matrix} = \sum_{i=i}^{N} \alpha_i H_i \Delta A_i \tag{a33}$$

Finally we want to express equation (a3) in vector form. This is not difficult since the operator $\int_c K(\underset{\sim}{x}_0 \underset{\sim}{x}) dA(\underset{\sim}{x}_0)$ acting on the function $B(\underset{\sim}{x}_0)$ is a linear transformation; that is, it obeys the following relation:

$$\int_c [\alpha B_1(\underset{\sim}{x}_0) + \beta B_2(\underset{\sim}{x}_0)] K(\underset{\sim}{x}_0, \underset{\sim}{x}) \, dA(\underset{\sim}{x}_0) = \alpha \int_c B_1(\underset{\sim}{x}_0) K(\underset{\sim}{x}_0, x) \, dA(\underset{\sim}{x}_0) + \beta \int_c B_2(\underset{\sim}{x}_0) K(\underset{\sim}{x}_0, x) \, dA(\underset{\sim}{x}_0) \tag{a34}$$

For any numbers α, β, and functions B_1, B_2.

The function $B(\underset{\sim}{x})$ is of course represented by the vector B and the operation $\int_c B(\underset{\sim}{x}_0) K(\underset{\sim}{x}_0, \underset{\sim}{x}) dA(\underset{\sim}{x})$ is represented by performing a linear transformation on B. A theorem states that any linear transformation on a vector in an N-dimensional vector space may be represented by the multiplication of the vector by an N x N matrix. One method of calculating the elements of this matrix is to consider the case in which each area ΔA_j is uniformly radiating a constant diffuse flux per unit area B_j. Then the cavity surface integral is broken into N integrals over the sub areas $\{\Delta A_j\}_{j=1}^{j=N}$ of the cavity. Equation (a3) becomes:

$$H(\underset{\sim}{x}) = \sum_{j=1}^{N} \int_{\Delta A_j} B_j K(\underset{\sim}{x}_0, \underset{\sim}{x}) \, dA(\underset{\sim}{x}_0) = \sum_{j=1}^{N} B_j \int_{\Delta A_j} K(\underset{\sim}{x}_0, \underset{\sim}{x}) \, dA(\underset{\sim}{x}_0) \tag{a35}$$

If we evaluate the average flux incident on each ΔA_i we have

$$H_i = \frac{\int_{\Delta A_i} H(\underset{\sim}{x}) dA(\underset{\sim}{x})}{\Delta A_i} \tag{a36}$$

This gives us

$$H_i = \sum_{j=i}^{N} B_j \frac{\int_{\Delta A_i}\int_{\Delta A_j} K(\underset{\sim}{x}_o, \underset{\sim}{x}) dA(\underset{\sim}{x}_o) dA(\underset{\sim}{x})}{\Delta A_i} \tag{a37}$$

If we define the matrix K by

$$K = (K_{ij}) = \frac{\int_{\Delta A_i}\int_{\Delta A_j} K(\underset{\sim}{x}_o, x) dA(\underset{\sim}{x}_o) dA(\underset{\sim}{x})}{\Delta A_i \Delta A_j} \tag{a38}$$

then we have, from equation (a37)

$$\underset{\sim}{H} = K(\Delta \underset{\sim}{A}\ \underset{\sim}{B}) \tag{a39}$$

and since $K(\underset{\sim}{x}_o, \underset{\sim}{x}) = K(\underset{\sim}{x}, \underset{\sim}{x}_o)$, we have $K_{ij} = K_{ji}$.

There is another useful way to look at this problem. Under the above conditions the total flux leaving the j-th sub area is $\Delta A_j B_j$ and the amount of flux reaching the i-th area from the j-th area is just $\Delta A_i K_{ij} \Delta A_j B_j$. so the fraction F_{j-i} of the flux leaving ΔA_j and arriving at ΔA_i is given by

$$\begin{aligned} F_{j-i} &= \Delta A_i K_{ij} \\ F_{i-j} &= \Delta A_j K_{ij} = \frac{\Delta A_j}{\Delta A_i} F_{j-i} \end{aligned} \tag{a40}$$

In matrix form this is

$$F = K\Delta A \tag{a41}$$

and equation (a3) has the analogue

$$\underset{\sim}{H} = F\underset{\sim}{B} \tag{a42}$$

The net local heat loss q_i at each ΔA_i on the cavity surface must be known for the thermal gradient calculation. One has the following equations:

$$\underset{\sim}{B} = \epsilon\sigma\underset{\sim}{T}^4 + \rho\underset{\sim}{H} \tag{a43}$$

$$\underset{\sim}{q} = \epsilon\sigma\underset{\sim}{T}^4 - \epsilon\underset{\sim}{H} \tag{a44}$$

$$\underset{\sim}{H} = K\Delta A\ \underset{\sim}{B} \tag{a45}$$

Combining (a43) with (a45), we obtain

$$\underset{\sim}{B} = \epsilon\sigma\underset{\sim}{T}^4 + \rho K \Delta A \underset{\sim}{B} \tag{a46}$$

This gives

$$(1 - \rho K \Delta A)\underset{\sim}{B} = \epsilon\sigma\underset{\sim}{T}^4 \tag{a47}$$

Physical reasoning tells us that the inverse matrix $(1 - \rho K \Delta A)^{-1}$ must exist, so we can write

$$\underset{\sim}{B} = (1 - \rho K \Delta A)^{-1} \epsilon\sigma\underset{\sim}{T}^4 \tag{a48}$$

The above equation is the solution for $\underset{\sim}{B}$ in terms of $\underset{\sim}{T}^4$ and geometry. To complete the derivation, we need an expression for $\underset{\sim}{q}$ in terms of $\underset{\sim}{B}$ and $\underset{\sim}{T}^4$. Equation (a43) gives us

$$\underset{\sim}{H} = \rho^{-1}(\underset{\sim}{B} - \epsilon\sigma\underset{\sim}{T}^4) \tag{a49}$$

Substituting this result into equation (a44) one obtains

$$\underset{\sim}{q} = \epsilon\sigma\underset{\sim}{T}^4 - \epsilon\rho^{-1}(\underset{\sim}{B} - \epsilon\sigma\underset{\sim}{T}^4) \tag{a50}$$

Taking $\underset{\sim}{B}$ from equation (a48), one obtains

$$\begin{aligned}\underset{\sim}{q} &= \epsilon\sigma\underset{\sim}{T}^4 - \epsilon\rho^{-1}[(1 - \rho K \Delta A)^{-1}\epsilon\sigma\underset{\sim}{T}^4 - \epsilon\sigma\underset{\sim}{T}^4] = \{1 - \epsilon\rho^{-1}[(1 - \rho K \Delta A)^{-1} - 1]\}\epsilon\sigma\underset{\sim}{T}^4 \\ &= \mathfrak{F}\,\epsilon\sigma\underset{\sim}{T}^4\end{aligned} \tag{a51}$$

where

$$\mathfrak{F} = \{1 + \epsilon\rho^{-1}[1 - (1 - \rho K \Delta A)^{-1}]\} \tag{a52}$$

Thus we can obtain the complete transfer solution matrix $\mathfrak{F}$ from a knowledge of K and ϵ. Equivalent prescriptions for obtaining this matrix have been given numerous times in the literature. In the present development the roles of matrix multiplication and inversion have been emphasized and the isomorphism between the vector $\underset{\sim}{\xi}$ and the matrix operation ϵ(or $\tau(\underset{\sim}{\xi})$) were described. This may help to clarify the mathematical situation because any equation involving expressions like those in equations (a1), (a2), or (a3) can be written down quickly in terms of vectors, linear transformations, linear functionals, or traces.

7.2 Angle Factors in a Cylindrical Cavity

The angle factors between various areas (ΔA_i) on the surface of a cylindrical cavity are relatively easy to evaluate. An expression for the fraction F_{i-j} of the diffuse flux leaving a given area, ΔA_i, which falls directly on any other area, ΔA_j, is needed. The cavity base is divided into a series of annular rings and the wall is divided into a series of cylindrical rings (Figure a1).

The angle factor between any two cylindrical rings of equal width, h, can be expressed as

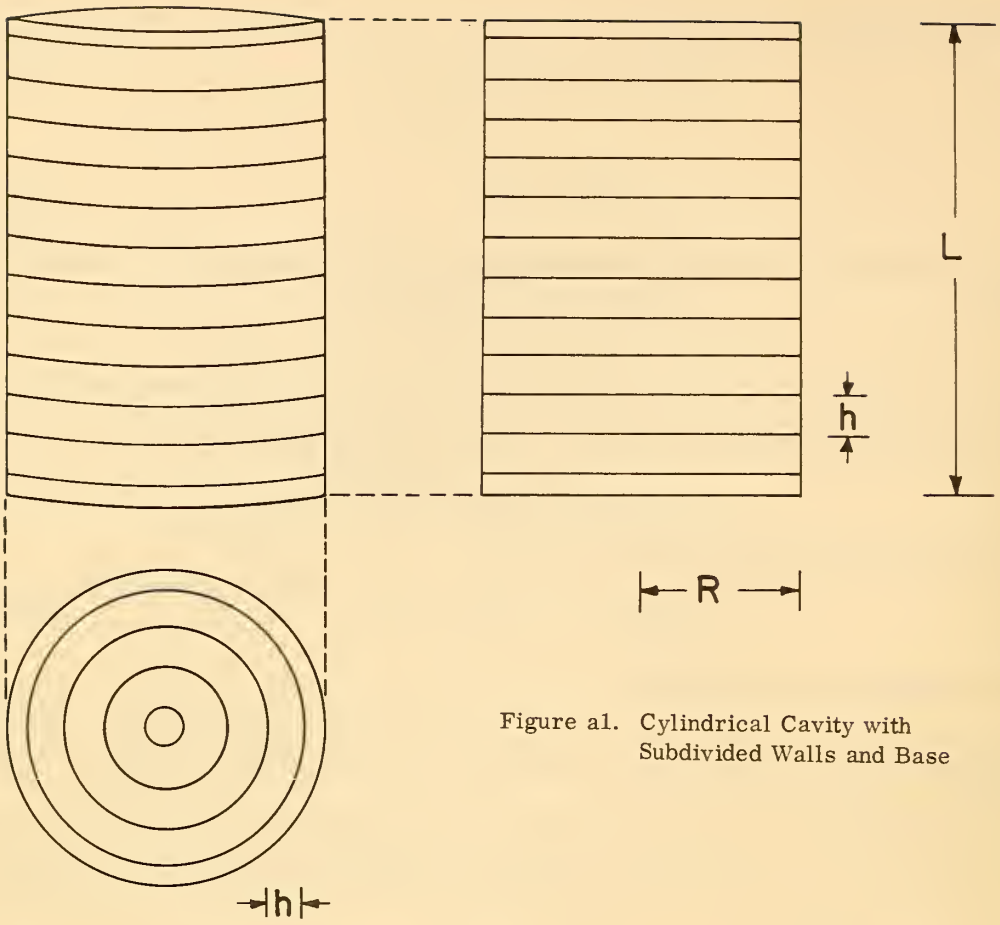

Figure a1. Cylindrical Cavity with Subdivided Walls and Base

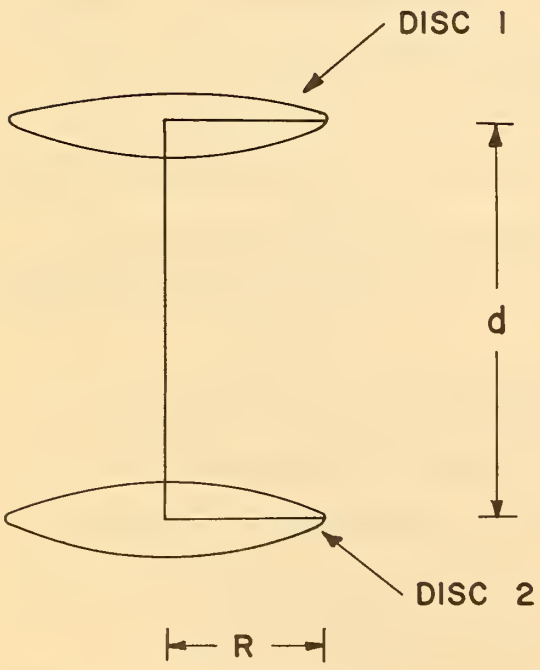

Figure a2. Coaxial Discs of Equal Radii

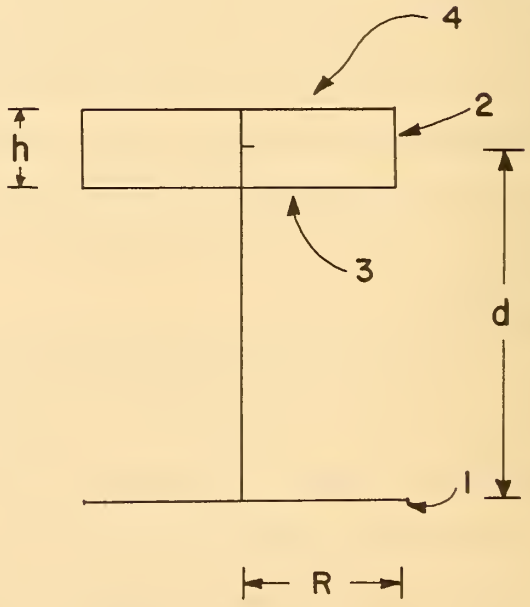

Figure a3. Section Through a Cylindrical Cavity

$$F_3(d,R,h) = F_2(d - 0.5h,R,h) - F_2(d + 0.5h, R, h) \quad (a53)$$

where d is the distance between the centers of the two rings, and R is the radius of the cylinder.

In the above equation, the function $F_2(d, R, h)$ is given by

$$F_2(d,R,h) = \frac{R}{2h} F_1(d,R,h) \quad (a54)$$

where

$$F_1(d,R,h) = F_0(d - 0.5h,R) - F_0(d + 0.5h,R) \quad (a55)$$

and

$$F_0(d,R) = \{d^2 + 2R^2 - (d^2 + 2R^2)^2 - 4R^4\}^{\frac{1}{2}} (2R^2)^{-1} \quad (a56)$$

The derivation of the above series of functional relationships proceeds as follows: $F_0(d, R)$ gives the fraction of the diffuse flux, leaving a circular disc of radius R, which is incident on a parallel circular disc of equal radius when the two discs are a distance d apart on the same axis (Figure a2). This equation is given by Walsh [22] for discs of unequal radii.

$F_1(d,R, h)$ is the fraction of the flux leaving disc 1 of radius R and reaching cylindrical ring 2 of radius R and width h whose center is located a distance d above the center of disc 1 (Figure a3). This fraction can be considered to be the difference between the fraction reaching disc 3 and that reaching disc 4 (Figure a3), and this is expressed in equation (a55). The fraction $F_2(d, R, h)$ of the flux leaving ring 2 and falling directly on disc 1 (in Figure a3) is easily calculated from equation (a40). Finally, the fraction of the flux leaving cylindrical ring 1 and reaching cylindrical ring 2 is given by $F_3(d, R, h)$ in equation (a53) above; $F_3(d, R, H)$ is expressed as the difference between the fraction leaving ring 1 and arriving at disc 3 and the fraction leaving ring 1 and arriving at disc 4 (Figure a4).

Similar reasoning gives the following series of functional relationships for the fraction $F_3'(R, h, d, r)$ of the flux leaving an annular ring 1 of width h and mean radius r on the base of a cylindrical cavity and falling incident on cylindrical ring 2 of width h located a mean distance d above the cavity base (Figure a5).

$$F_3'(R,h,d,r,h) = F_2'(R,d - 0.5h,r,h) - F_2'(R,d + 0.5h,r,h) \quad (a57)$$

$$F_2'(R,h,r,h) = \frac{R^2 F_1'(R,d,r,h)}{[(r + 0.5h)^2 - (r - 0.5h)^2]} \quad (a58)$$

$$F_1'(R,d,r,h) = F_0'(R,r + 0.5h,d) - F_0'(R, - 0.5h,d) \tag{a59}$$

$$F_0'(d,R,r) = \{d^2 + R^2 + r^2 - [(d^2 + r^2 + R^2)^2 - 4R^2r^2]^{\frac{1}{2}}\}(2R^2)^{-1} \tag{a60}$$

The fraction $F_4'(R, h, d, r, h)$ of the flux leaving cylindrical ring 2 of the width h located a mean distance d above the base of the cylindrical cavity and incident on an annular ring of width h and mean radius r on the cavity base is given by

$$F_4'(R,h,d,r,h) = \frac{[(r + 0.5h)^2 - (r - 0.5h)^2]}{2Rh} F_3'(R,h,d,r,h) \tag{a61}$$

These functional relationships have been incorporated into a subroutine of the computer program that will calculate the temperature distribution in the cylindrical specimen. This subroutine is currently under development.

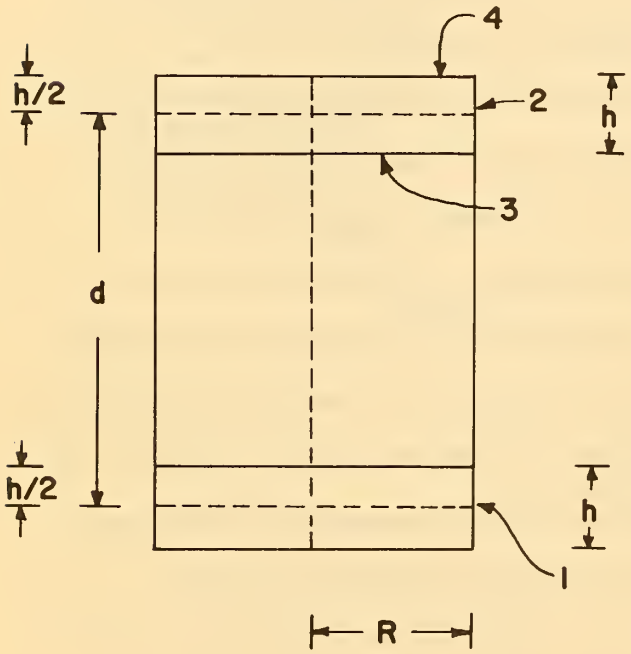

Figure a4. Section Through a Cylindrical Cavity

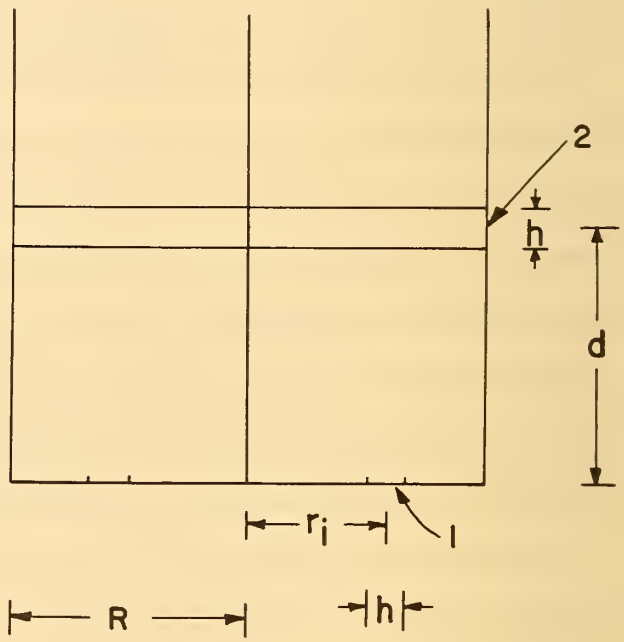

Figure a5. Section Through a Cylindrical Cavity

8. Appendix II

Measurements were made of the total normal emittance of several materials by the deep cavity and center post modifications of the shallow cavity technique after the end of the period covered by this report. In order to make the best values for these properties available without delay, the data are included in this appendix.

The emittance of the tungsten used for the susceptor was measured by the deep hole method. These data are presented in Figure a6. The hole was coated with silicon carbide to make its emittance nearly one. Since tungsten is a metal, it is not translucent and the temperature is nearly uniform throughout the sample. The total error in this measurement is estimated to be less than 2%.

The data for alumina, thoria, magnesia and zirconia obtained by the center post and deep cavity procedures are compared in figures a7, a8, a9 and a10 with data obtained by the shallow cavity procedure, and by integration of spectral data on similar specimens measured by the rotating cylinder procedure. Several trends are evident. In general, the shallow cavity procedure gave the highest values of emittance, and the comparison post method gave the lowest values.

Except for the case of thoria, where the specimens measured by the rotating cylinder method were appreciably different from those measured by the other procedures, the data obtained by integration of spectral values are only slightly higher than those obtained by the comparison post method.

All of the data have been corrected for the optical scattering error. The shallow cavity data have not been corrected for either the translucency error or the temperature difference error. The deep cavity data should be essentially free from the translucency error, but have not been corrected for the temperature difference error. The comparison post data should be completely free from the translucency error, and have been corrected for the temperature difference error on the basis of optical pyrometer temperature measurements.

It can be concluded from the figures that the data obtained by the comparison post technique are more nearly accurate than those obtained by the shallow cavity or deep cavity procedures.

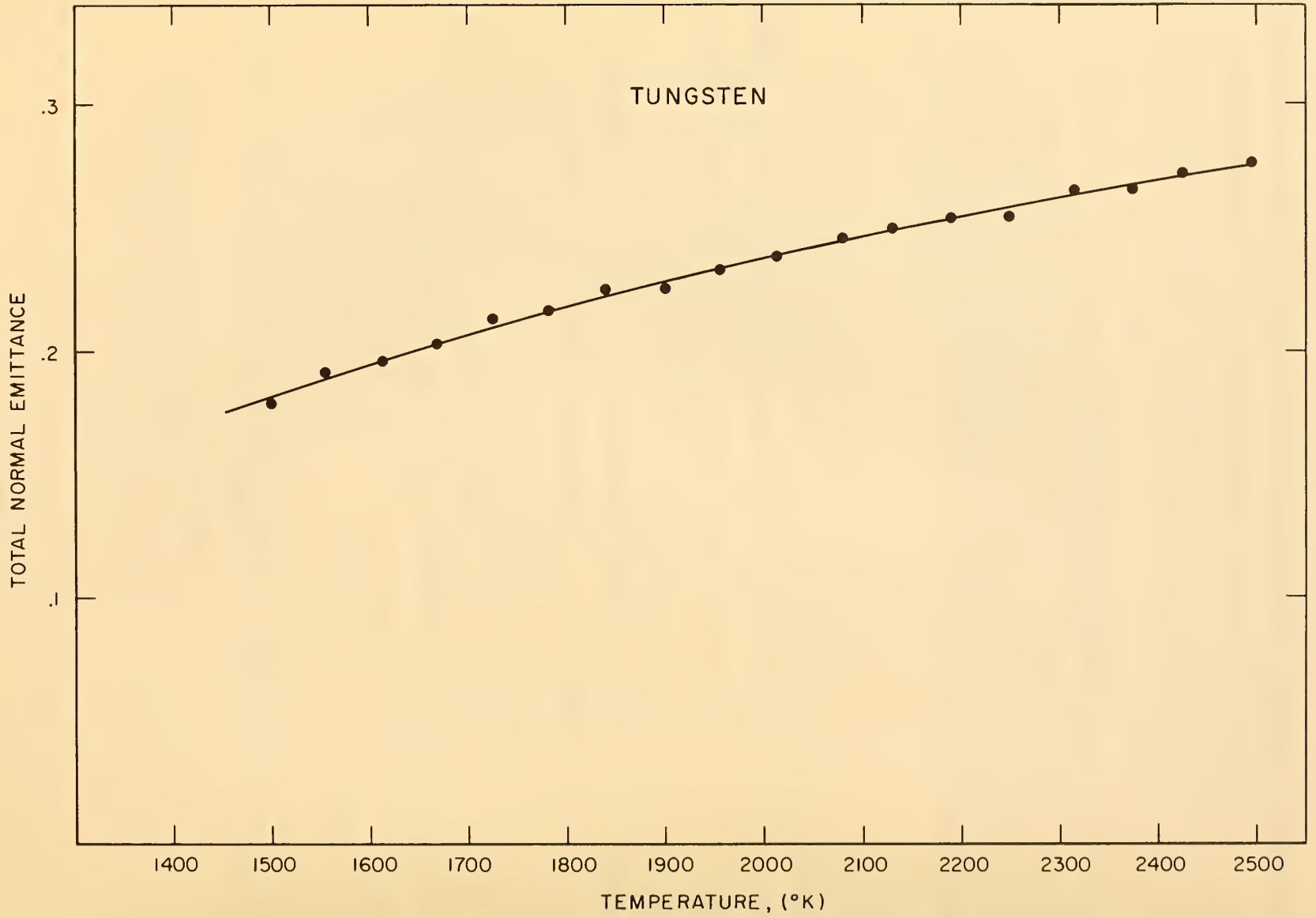

Figure a6. Total Normal Emittance of Tungsten

The ceramic oxide specimens were obtained from the Laboratory Equipment Corporation, St. Joseph, Michigan. A chemical analysis was supplied by the vendor and is presented in Table 1B. The porosity of the specimens was alumina 30%, Thoria 13%, Magnesia 30% and Zirconia 20% by volume. The tungsten was supplied by Wah Chang Company, New York, N. Y.

Table 1B. Vendor's Chemical Analysis of Specimen Materials in Percentage by Weight

	Alumina[a]	Thoria[b]	Magnesia	Zirconia
Al_2O_3	99. +	---	0. 1	0. 15
ZrO_2+HfO_2	---	---	---	94. 2
ThO_2	---	99. +	---	---
SiO_2	0. 10	0. 05	0. 4	0. 60
TiO_2	---	---	---	0. 30
CaO	0. 07	trace	0. 1	4. 50
MgO	---	0. 02	99. 2	0. 07
Fe_2O_3	0. 40	---	0. 1	0. 10

a/ Also, 0. 02% Na_2O%.

b/ Also, trace amounts of the oxides of phosphorus, iron, and the rare earths as well as a minor amount of alkali oxides which was expressed in the analysis as 9. 10 % of combined Na, K, and Li.

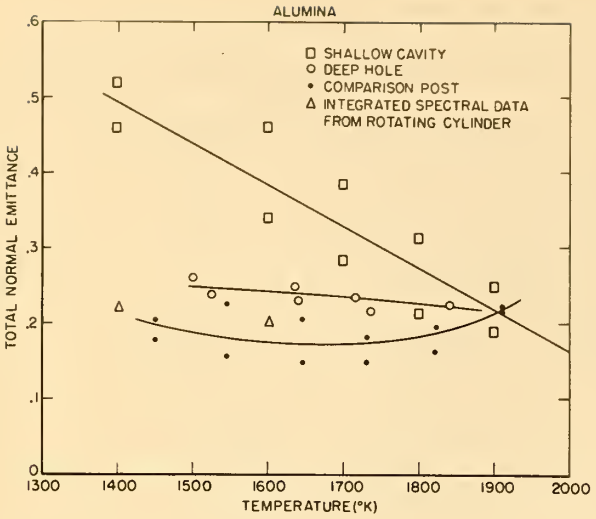

Figure a7. Total Normal Emittance of Alumina

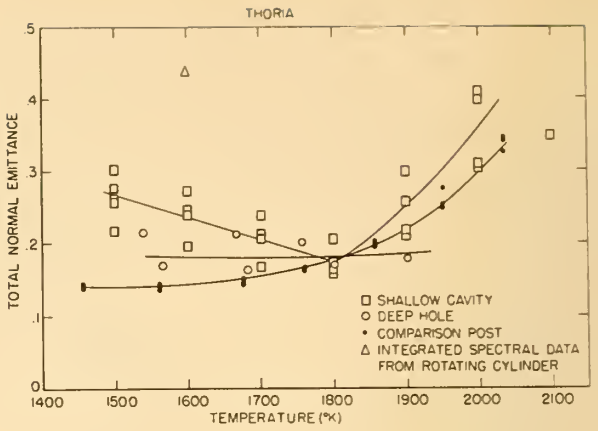

Figure a8. Total Normal Emittance of Thoria

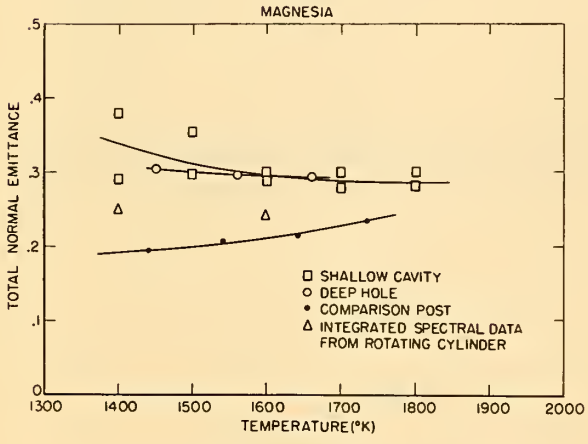

Figure a9. Total Normal Emittance of Magnesia

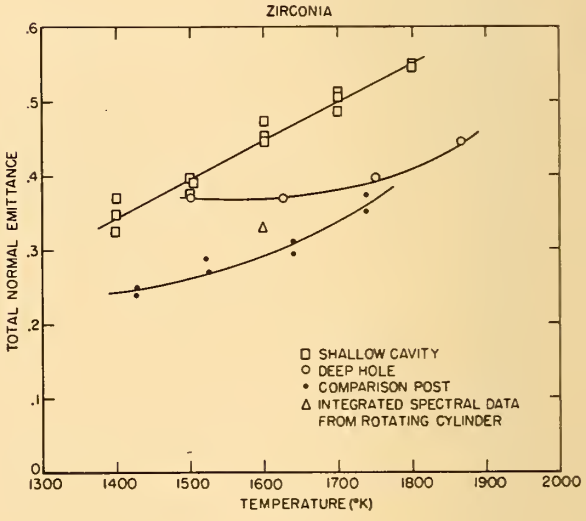

Figure a10. Total Normal Emittance of Zirconia

* U.S. GOVERNMENT PRINTING OFFICE: 1967—251-024/65

U.S. DEPARTMENT OF COMMERCE
WASHINGTON, D.C. 20230

OFFICIAL BUSINESS

POSTAGE AND FEES PAID
U.S. DEPARTMENT OF COMMERCE